

Study, Analysis, and Validation of a Specific Two-fluid Model for Dispersed Two-Phase Flow

by

Mehrdad Khezrian

A thesis
presented to the University of Waterloo
in fulfillment of the
thesis requirement for the degree of
Master of Applied Science
in
Chemical Engineering

Waterloo, Ontario, Canada, 2021

© Mehrdad Khezrian 2021

Author's Declaration

I hereby declare that I am the sole author of this thesis. This is a true copy of the thesis, including any required final revisions, as accepted by my examiners.

I understand that my thesis may be made electronically available to the public.

Abstract

Multiphase flows are commonly found and have a significant role in different processes in the energy, environmental, biological, and pharmaceuticals industries. The behavior of multiphase flows is very complicated due to their multiphysics nature and the fact that they involve more than one simultaneous physical field. An understanding of this behavior is vital for designing and operating process equipment in the aforementioned industries. While experimentation can be a useful method of acquiring this information, its limitations make it impractical in many cases. Specifically, experimental approaches can be time-consuming, expensive, and, in some cases, are infeasible.

Computational fluid dynamics (CFD) can be a more feasible option. However, the accuracy of CFD simulations rely heavily on the model used to represent the underlying physical phenomena, closures introduced, and numerical methods employed to solve the model. As a result, considerable effort has been put into developing multiphase flow models in the literature. In general, the validity of different variations of the two-fluid model could be examined from two points of view: (i) physical fidelity of the canonical form of the model and (ii) accuracy of the closures used to describe the interphase momentum exchange term. In the two-fluid model canonical form, a key point to consider is whether or not molecular fluxes (stress, etc.) appear in the dispersed phase momentum equation. Furthermore, many different closure terms are used in the literature for performing simulations without conclusive efforts to validate them.

In this research, most of the effort has been devoted to addressing these issues. First, a less-studied variation of the two-fluid introduced by Brennen, which has a more physically-informed mathematical derivation is introduced and discussed. Having established the canonical form of the Euler-Euler model, the interphase momentum exchange term is studied. Three closures supported by theoretical derivations are analyzed through scaling analysis and simulation. This analysis involves three different multiphase flow regimes present in industrial processes: bubbly flow, particulate flow, and flow of microorganisms in liquid. Finally, based on these analyses, the dispersion force was determined to be the most significant of the three closure terms, and as a result, added to the model. Eventually, the final form of the Brennen two-fluid model and the dispersion force as momentum exchange term is formulated and used for simulation and validation.

While not conclusive, simulation results are promising where, for a bubbly flow test case, the Brennen model with dispersion achieved better accuracy than the well-known standard version of the two-fluid model, especially in areas with high velocity magnitude. Additionally, using the dispersion force, the nonphysical behavior in the regions with high

gradient in volume fraction is removed, and smoother results for the volume fraction of dispersed phase are obtained.

Acknowledgements

First of all, I would like to thank my supervisor, Professor Nasser Mohieddin Abukhdier, for his mentorship, guidance, and support through this project and this opportunity.

Thank you to all members of the COMPHYS research group for helping to maintain a sense of community while working from home during a pandemic. Specific thanks to James Lowman, Dr. Tanyakarn Treeratanaphitak, and Alex Vasile for their help and the time they devoted to the progress of this work, and Sajeda Mokbel as a great office mate.

Additional thanks and deepest gratitude to my family, Sara, and all my friends. None of this would be possible without their encouragement and support.

I acknowledge and thank the University of Waterloo for the Engineering Excellence Fellowship and GRS funding and the RBC Water Scholars Graduate Entrance Scholarship. Finally, I thank Compute Canada for the use of its computational resources.

Dedication

To my parents.

Table of Contents

List of Tables	x
List of Figures	xi
1 Introduction	1
1.1 Research Motivation	1
1.2 Objectives	3
1.3 Structure of Thesis	4
2 Background and Literature Review	5
2.1 Classification of two-phase flow	5
2.2 Different methods of averaging	8
2.3 Derivation of the two-fluid model using time averaging	9
2.3.1 Conservation of Mass	10
2.3.2 Conservation of Momentum	11
2.4 Derivation of the two-fluid model using volume averaging	14
2.4.1 Derivation using a phase indicator function	14
2.4.2 Derivation using cell averaging method	19
2.5 Derivation of the two-fluid model using kinetic theory of gases and ensemble averaging	23
2.5.1 Kinetic theory principles	24

2.5.2	Boltzmann Transport Equation	24
2.5.3	Maxwell Transport Equation	25
2.6	Derivation of the two-fluid model using a modified control volume	28
2.6.1	Conservation of mass	28
2.6.2	Conservation of momentum	29
3	Interphase Momentum Exchange Terms	35
3.1	Introduction	35
3.2	Interphase momentum exchange	36
3.2.1	Drag Force	37
3.2.2	Lift Force	40
3.2.3	Virtual Mass Force	42
3.2.4	Wall Lubrication Force	43
3.2.5	Interfacial Pressure	43
3.3	Kinetic Theory-Based Closures	45
3.3.1	Bubble Pressure and Effective Stress	46
3.3.2	Dispersion Force	48
4	Scaling Analysis of Closure Terms	51
4.1	Closures derived based on kinetic theory	51
4.2	Conservation of Mass	53
4.2.1	Bubbly Flow	54
4.2.2	Liquid/Dispersed Microorganism Flow	54
4.2.3	Particulate Flow	54
4.3	Conservation of Momentum	55
4.3.1	Bubbly Flow	56
4.3.2	Liquid/Dispersed Microorganism Flow	58
4.3.3	Particulate Flow	59
4.4	Discussion of Scaling Analysis Results	60

5	Results and Validation	63
5.1	The final form of the two-fluid model	63
5.2	Test Case: Laboratory-scale bubble column	64
5.2.1	Geometry, mesh, and simulation condition	65
5.3	Comparison of 2-D simulation results with a reference solution	67
5.3.1	The dispersed phase volume fraction fields	67
5.3.2	The continuous phase vertical velocity	68
5.4	Validation and comparison of 3-D simulation results with a reference solution	69
5.4.1	The dispersed phase volume fraction field without dispersion force .	69
5.4.2	Vertical dispersed phase velocity without dispersion force	70
5.4.3	Vertical continuous phase velocity without dispersion force	71
5.4.4	The dispersed phase volume fraction field with dispersion force . . .	72
5.4.5	Validation of vertical continuous phase velocity with experimental results	72
5.5	Influence of dispersion force on simulation results	74
5.5.1	Instantaneous dispersed phase volume fraction field	74
5.5.2	Time-averaged dispersed phase volume fraction field	75
5.5.3	Validation of influence of dispersion force with experimental results	77
5.6	Mesh dependency of the solutions	78
5.7	Summary	79
6	Conclusion and Future Work	80
6.1	Conclusion	80
6.2	Future Work	81
	References	83
A	Source Code	89
A.1	Constant Dispersion Model	89

List of Tables

3.1	The drag coefficient for different flow regimes [1]	39
4.1	Properties of the dispersed phase in different flow regimes	52
4.2	The order of magnitude of closure terms in different multiphase flow regimes	61

List of Figures

2.1	Classification of two-phase flow [2]	6
2.2	Flow regime map in a pipeline [3]	7
2.3	Flow regime map for a bubble column [4, 5]	7
2.4	Various flow regimes in bubble column reactors [4]	8
2.5	The scale of the system, characteristic lengths, and averaging volume of each phase [6]	20
2.6	The modified control volume used in derivation of the momentum equations	30
3.1	Drag coefficients of smooth, axially symmetric bodies [7]	38
3.2	Schematic diagram of a spherical particle in a shear flow [2]	41
3.3	Schematic of the particle with the virtual mass added to it (the blue region) [8]	42
3.4	Effect of the wall lubrication force on volume fraction (α_d): Comparison between the simulation and experimental results	44
3.5	Schematic of the a)drag, b)lift, c)pressure gradient, d)virtual mass, e)wall lubrication force on the dispersed phase. [9]	45
4.1	Volume fraction results in a bubble column with and without the dispersion force. [10]	62
5.1	The bubble column configuration and the position of sparger [11]	65
5.2	The geometry of 2-D [12] and 3-D test cases used for running simulation	66
5.3	Time-averaged volume fraction field of dispersed phase: Brennen's model (left), Ishii's model (right)	68

5.4	Comparison of the time-averaged continuous phase velocity at heights of 13 cm(left), 25 cm (middle), and 37 cm (right)	69
5.5	Time-averaged volume fraction field of dispersed phase: Brennen’s model (left), Ishii’s model (right)	70
5.6	Comparison of the time-averaged dispersed phase velocity at heights of 13 cm (left), 25 cm (middle), and 37 cm (right)	71
5.7	Comparison of the time-averaged continuous phase velocity at heights of 13 cm (left), 25 cm (middle), and 37 cm (right)	71
5.8	Time-averaged volume fraction field of dispersed phase: Brennen’s model (left), Ishii’s model (right)	72
5.9	Validation of the time-averaged continuous phase velocity at heights of 13 cm (left), 25 cm (middle), and 37 cm (right)	73
5.10	The volume fraction of dispersed phase field at the time: t=2 s, with (left) and without (right) dispersion force	75
5.11	The time-averaged volume fraction of dispersed phase field with (left) and without (right) dispersion force	76
5.12	The time-averaged volume fraction of dispersed phase at height 25 cm with and without dispersion force	77
5.13	Validation of the time-averaged continuous phase velocity at heights of 13 cm (left), 25 cm (middle), and 37 cm (right) with and without dispersion force	78
5.14	Comparison of the simulation results with mesh refinement	79

Chapter 1

Introduction

1.1 Research Motivation

Multiphase flows involve the simultaneous flow of a mixture of phases [13] and are commonly found in different industrial and natural processes. Consequently, understanding of multiphase flow phenomena is of significant importance for the design and operation of these processes and for increased fundamental understanding. For example, liquid/dispersed gas multiphase flows are present in bubble columns [14], nuclear reactors [15], and horizontal pipelines [16] in the energy industry. Multiphase flow systems are also common in chemical and biochemical reactors in biological, biotechnological, and pharmaceuticals industries [17]. Moreover, in fluidized bed reactors, three-phase gas-liquid-solid flows are prevalent [18], and they have a significant role in the environmental and oil & gas industries.

The hydrodynamic behavior of multiphase flows is very complex and manifested in many different observed flow regimes. Yet, the understanding and control of this behavior is vital for designing and operating process equipment.

Use of experimentation is one approach to increase our understanding of multiphase flows. However, this class of approaches is infeasible for many practical operating conditions. Additionally, experiments can be costly, time-consuming, and involve potential safety issues. Alternatively, computational fluid dynamics (CFD) is desirable due to the feasibility of access for many practical operating conditions, reduced cost, and elimination of safety issues.

Using CFD simulations, information such as pressure drop and velocity distribution within a multiphase flow is accessible, along with other observations that are infeasible to

access experimentally. CFD simulations may also be used for simulation-based prototyping to compare different designs of particular piece of equipment before physical prototyping. Furthermore, CFD is widely being used in research to validate the accuracy of newly developed models through comparison to complex and time-evolving experimental observations.

The accuracy of CFD simulations is highly dependent on the theory, model, and numerical methods used. As a result, significant effort has been made in the literature to develop multiphase flow models [2, 19, 17, 20, 21] valid for different multiphase flow regimes and involving different degrees of description of the phases. Simultaneously, simulation-based research on multiphase flows has increased recently due to the increasing availability of computational resources. However, in many ways, progress is still restricted by lack of detailed understanding of microscopic and macroscopic processes underlying multiphase flows. There are many different multiphase flow regimes type that motivates the development of models that are specific to them and a universal model for multiphase flows has not been derived yet [22]. Therefore, choosing a suitable model, which is usually a function of the system, is very important and affects the accuracy and computational complexity of simulations.

Dispersed two-phase flows are perhaps the most prevalent multiphase flow type observed in the industry, and it is encountered in almost any of the cases mentioned above [22]. In addition, the equations and relations describing the hydrodynamics of two-phase flow are similar and can be extended to multiphase flow with more than two phases. Therefore, this research focuses on the dispersed two-phase multiphase flow regime.

Current approaches for modelling dispersed two-phase flow fall into two main categories: Euler-Lagrange and Euler-Euler (two-fluid) models. Both approaches treat the continuous phase as a continuum, with them differing in how the dispersed phase is treated. Euler-Lagrange models treat the dispersed phase as a set of discrete particles whose motion is governed by individual equations of motion. On the other hand, the Euler-Euler approach averages interface-capturing multiphase models resulting in continuum approximations for both the continuous and dispersed phases [22, 23].

In the Euler-Lagrange model, the equation of motion for each dispersed phase element is solved through the flow domain. Therefore, the conservation equations of each individual element are expressed in a coordinate that follows the element trajectory. The conservation of momentum equation (equation of motion) for each element, simply relates the rate of change of the element velocity to sum of the forces acting on it:

$$\rho_d \frac{d\mathbf{u}_d}{dt} = \sum \mathbf{F} \quad (1.1)$$

This theoretical approach has several benefits stemming from the ability to differentiate

particles properties (size, shape, *etc.*). However, problems arise with the use of Euler-Lagrange model due to the very large number of particles present in the dispersed phase for many industrially-relevant multiphase flows. Hence, a high computational cost restricts the use of this method in most cases [23].

The Euler-Euler (two-fluid) model, in contrast, approximates the dispersed phase elements as a continuum by applying a suitable averaging procedure. As a result, the computational complexity involved in solving this model is reduced significantly compared to interface-capturing and Euler-Lagrange models. Although the accuracy is decreased compared to Euler-Lagrange models, it is acceptable in many cases, in order to perform simulations on relevant experimental and industrial scales. The resulting mathematical equations are similar to the single-phase continuum equations but contain a set of additional terms that account for the interactions between the two phases and couples the equations of different phases together. These interaction terms or closures, *e.g.*, drag, virtual mass, lift, are included in a single term called interphase momentum exchange (or transfer) which appears on both phases governing equations. It has been shown that the selection of these momentum exchange terms can affect the simulation results significantly [24].

The two-fluid model itself can be derived using different methods. The most common are time-averaging [2], volume averaging [25], and kinetic theory & ensemble (or statistical) averaging [20]. Overall, different variations of the two-fluid model and their physical fidelity could be analyzed from two points of view: that of the canonical form of the model and that of the closures used in the momentum exchange term. Little research has been done using the former view, with the majority focusing on the latter view. For instance, the presence of molecular fluxes (hydrodynamic and hydrostatic stress) in the canonical form of the two-fluid model is unclear from a physical point of view.

1.2 Objectives

The overall objective of this work is to identify and/or develop a two-fluid model which has a physically consistent mathematical derivation along with interphase momentum transfer closures which are motivated by physical accuracy and purely mathematical considerations. This variation of the two-fluid model is then be validated with experimental results and compared to other variations via simulation. To achieve that, different derivation methods of the two-fluid model, including time and volume averaging, kinetic theory and ensemble averaging, and a modified time/volume averaging method are first introduced and reviewed. After determining the most physically consistent canonical form of the model based on the

above study, three closures used as interphase momentum exchange term are studied and analyzed, namely using dimensional analysis for three different multiphase flow regimes, *e.g.*, for bubbly flow, particulate flow, and dispersed microorganism/liquid flow. Finally, simulations are run in order to validate the resulting model against experimental results as well as reference solutions.

1.3 Structure of Thesis

This thesis is organized into six chapters: Chapter 2 - Background and literature review, Chapter 3 - Interphase momentum exchange term, Chapter 4 - Scaling analysis of the closures, Chapter 5 - Results and validation, Chapter 6 - Conclusion and future work.

Chapter 2 explains the background knowledge required to understand this work and also presents a literature review on different methods of derivation of two-fluid model. This chapter starts by going through the different types of multiphase flow and then goes through the derivation of the canonical form of the two-fluid model using time-averaging [2], volume-averaging [25, 6], kinetic theory and ensemble averaging [20], and a modified volume-averaging [21]. It also discusses the physical fidelity of the model derived from these methods.

Chapter 3 discusses the momentum exchange term and reviews different closures used for the two-fluid model. Other than the well-known closures such as drag, lift, virtual mass, *etc.*, three less studied closures are introduced and discussed. These closures are different from many others in that their derivation is supported by the theoretical analysis of the kinetic theory.

In Chapter 4, more analysis on these three closures for three multiphase flow regimes, namely bubbly flow, dispersed microorganisms in liquid, and solid particles in liquid flow is performed. Using scaling analysis, the most significant of these three closures is determined for the three multiphase flow regimes and is added to the model introduced in Chapter 2.

Chapter 5 introduces the proposed form of the two-fluid model based on the analysis and discussion from the previous chapters. Subsequently, a test case will be presented in order to validate the results of simulations from our model with experimental results and benchmark them with existing `OpenFOAM` two-fluid solver, `twoPhaseEulerFoam` that are based on the standard version of the two-fluid model.

Finally, chapter 6 summarizes the conclusions of this work and provides recommendations for future work.

Chapter 2

Background and Literature Review

2.1 Classification of two-phase flow

There is a wide range of multi-phase flow regimes and patterns. These can then be divided into a few recognizable classes. A multiphase flow can be classified by its physical state of constituent components and by the topology of its interfaces. Consequently, a two-phase flow can be classified into gas-solid, gas-liquid, liquid-solid, or liquid-liquid in the case of two immiscible liquids. The flow can also be classified based on its topology as separated, dispersed, or mixed. Separated flows include free-surface flows, for example, a stratified flow in a duct, where two phases are separated by a continuous interface. Dispersed flows consist of a dispersed phase consisting of particles, droplets, or bubbles suspended within a continuous phase. Transitional flows are between the two forms described above. In [Figure 2.1](#), these regimes and some of the sub-regimes that are relevant to them are depicted.

Classification based on interface structures and the topographical distribution of each phase is much more difficult since these structures continuously change due to motion and transformation between phases. Several factors can influence the transition between the phases, including geometry, flow rate, surface tension, etc. Furthermore, more than one flow pattern may exist within a given system.

To describe the main flow patterns and their transitions, experimental observations have been employed to construct two-dimensional flow regime maps that relate the flow pattern to its properties. [Figures 2.2](#) and [2.3](#) show the flow regime map for horizontal flow in a pipeline and vertical flow in a bubble column as a function of the superficial gas velocity and column diameter, respectively.

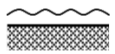
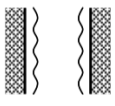

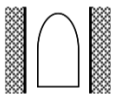
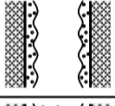
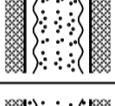
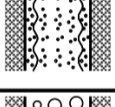
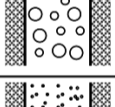
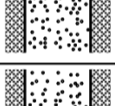

Class	Typical regimes	Geometry	Configuration	Examples
Separated flows	Film flow		Liquid film in gas Gas film in liquid	Film condensation Film boiling
	Annular flow		Liquid core and gas film Gas core and liquid film	Film boiling Boilers
	Jet flow		Liquid jet in gas Gas jet in liquid	Atomization Jet condenser
Mixed or Transitional flows	Cap, Slug or Churn-turbulent flow		Gas pocket in liquid	Sodium boiling in forced convection
	Bubbly annular flow		Gas bubbles in liquid film with gas core	Evaporators with wall nucleation
	Droplet annular flow		Gas core with droplets and liquid film	Steam generator
	Bubbly droplet annular flow		Gas core with droplets and liquid film with gas bubbles	Boiling nuclear reactor channel
Dispersed flows	Bubbly flow		Gas bubbles in liquid	Chemical reactors
	Droplet flow		Liquid droplets in gas	Spray cooling
	Particulate flow		Solid particles in gas or liquid	Transportation of powder

Figure 2.1: Classification of two-phase flow [2]

The major limitation of flow regime maps is that they are only useful for the exact conditions under which they are derived and they cannot be used to predict flow patterns for other situations. Additionally, while the maps represent different flow patterns by

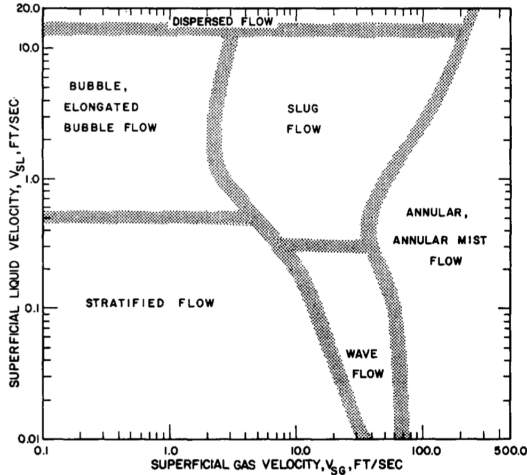


Figure 2.2: Flow regime map in a pipeline [3]

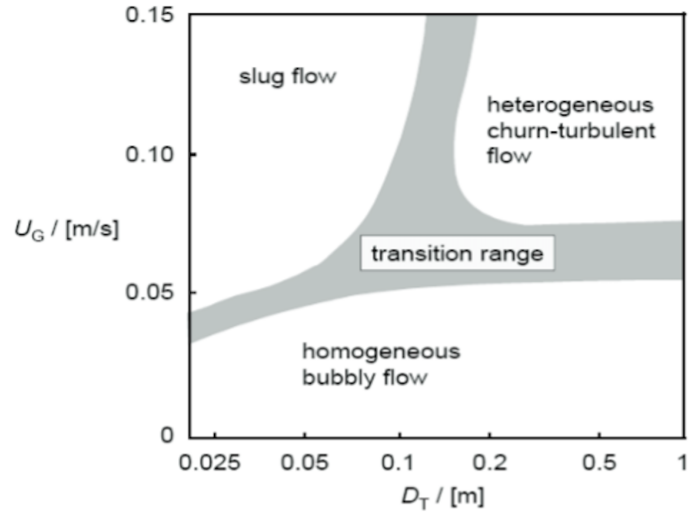


Figure 2.3: Flow regime map for a bubble column [4, 5]

separating them with thin lines, the transition between them occurs gradually over a range of flow rates, which impacts their usefulness [22].

Despite the wide variety of multiphase flow regimes and patterns, the same fundamental methods are used to derive the governing equations of the flow, which are conservation of mass, momentum, and energy. Moving away from empirical correlations based on experimental data in favor of more generally applicable and accurate mathematical models, which are based on these fundamental laws had a key role in the progress of predictive techniques for flow behavior.

Dispersed two-phase flow is perhaps the most prominent regime in industry, and it is observed in energy and environment, biological, and chemical processes, as described in the previous chapter. Moreover, the equations and correlations describing the hydrodynamics of two-phase flows are similar and can be extended to multiphase flow with more than two phases. Therefore, the present work focuses on techniques and models applicable to dispersed two-phase flow.

In particular, the rest of this chapter introduces different averaging methods used for derivation of the governing equations of dispersed two-phase flow which are time-averaging, volume-averaging, kinetic theory and ensemble averaging. Then the derivation of the model using these methods will be scrutinized and discussed, and finally, the model with the most physical validity will be selected and adopted for the rest of this study.

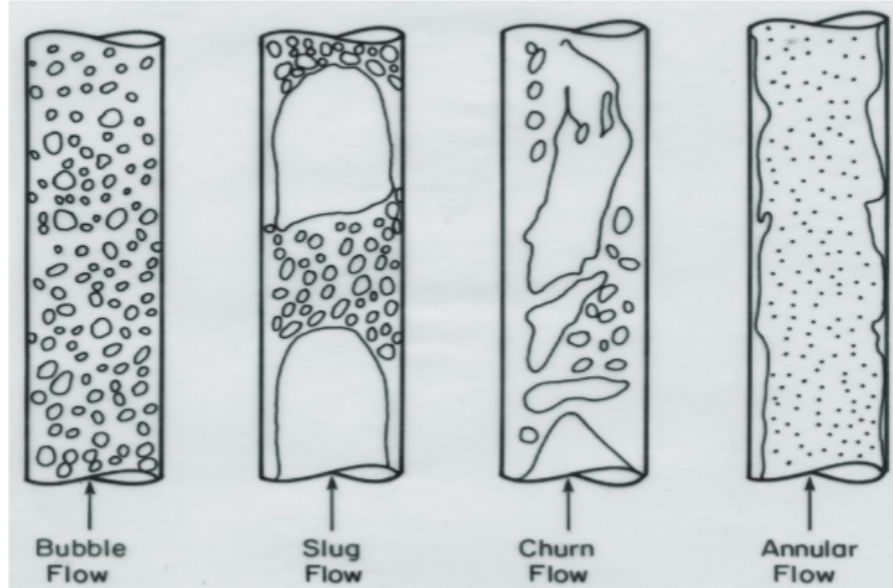


Figure 2.4: Various flow regimes in bubble column reactors [4]

2.2 Different methods of averaging

As with the continuum mechanics framework for deriving properties of single-phase flow, multiphase flow models are expected to be derived using appropriate field and constitutive relations. However, the formulation based on the local instantaneous variables encounters overwhelming difficulties due to the complex nature of multiphase flow arose from the existence of a large number of deformable and moving interfaces, the existence of the fluctuations in variables, and significant discontinuities in the properties at the interface. Consequently, the derivation of governing equation for multiphase flow is remarkably complicated when compared to single-phase [2].

In order to address these mathematical and numerical difficulties, averaging methods are used to eliminate the local instant fluctuations that are rarely required for engineering problems and derive the flow's macroscopic properties. In fact, averaging acts as a low-pass filter that eliminates the unwanted high frequency signals from the local instant fluctuations. Nonetheless, in the formulation based on averaging, it is important to consider the statistical properties of these fluctuations that affect macroscopic phenomena [1].

As mentioned before, time, volume, and ensemble averaging are used to derive the

two-fluid model which is defined as follows [2]:

Time averaging:

$$\bar{\phi} = \frac{1}{\Delta t} \int_{\Delta t} \phi dt \quad (2.1)$$

Volume averaging:

$$\langle \phi \rangle = \frac{1}{\Delta V} \int_{\Delta V} \phi dV \quad (2.2)$$

Ensemble averaging:

$$\langle \phi \rangle_E = \frac{1}{N} \sum_{n=1}^N \phi_n \quad (2.3)$$

where Δt and ΔV are the volume averaging and time averaging domains and N is the total number of realizations in the ensemble ($N \rightarrow \infty$) and ϕ_n is the value of ϕ for a particular realization.

For time and volume averages to be rigorous and meaningful, they must be subject to specific constraints, and the averaging domains must be clearly defined. Consequently, it is extremely important to take into account the particle time and length scales as well as the turbulence time and length scales. In order to obtain a meaningful average, the averaging time/volume domain should be larger than the time/length scale of particles while smaller than the time/length scale of macroscopic flow features [22].

2.3 Derivation of the two-fluid model using time averaging

We shall start the study of the derivation of the two-fluid model by going through Ishii et al.'s derivation in Thermo-Fluid Dynamics of Two-Phase Flow using time averaging [2]. The general balance of quantity ψ is given by the following equation:

$$\frac{\partial(\rho\psi)}{\partial t} + \nabla \cdot (\rho\psi\mathbf{v}) + \nabla \cdot \mathbf{J} - \rho\phi = 0 \quad (2.4)$$

The first term on the left-hand side is the time rate of change of the quantity per unit volume, and the second term is the rate of convection per unit volume. In the third and fourth terms, \mathbf{J} and ϕ , are the generalized tensor flux (diffusion) and the quantity's source term, respectively. The time averaging operator in the limit of zero thickness of interface is defined as follows:

$$\bar{F}(\mathbf{x}_0, t_0) \equiv \lim_{\delta \rightarrow 0} \frac{1}{\Delta t} \int_{[\Delta t]_T} F(\mathbf{x}_0, t) dt \quad (2.5)$$

where $\delta \rightarrow 0$ specifies that the interfacial region is approximated with a singular surface with a thickness of zero. Applying the time averaging operator on Equation 2.4, the following equation is going to be obtained for each phase:

$$\frac{\partial(\alpha_k \bar{\rho}_k \widehat{\mathbf{v}}_k)}{\partial t} + \nabla \cdot (\alpha_k \bar{\rho}_k \widehat{\psi}_k \widehat{\mathbf{v}}_k) = -\nabla \cdot [\alpha_k (\bar{\mathbf{J}}_k + \mathbf{J}_k^T)] + \alpha_k \bar{\rho}_k \widehat{\phi}_k + I_k \quad (2.6)$$

where $\bar{\rho}_k$ and $\bar{\mathbf{J}}_k$ are the time-averaged phasic average density and time-averaged phasic tensor flux, α_k is the time-averaged phase fraction, $\widehat{\mathbf{v}}_k$ is the time-averaged mass-weighted mean phase velocity, and \mathbf{J}_k^T is turbulent flux. I_k is the interfacial source of the quantity ψ for phase k and its definition is [2]:

$$I_k \equiv -\frac{1}{\Delta t} \sum_j \left\{ \frac{1}{v_n^{int}} \mathbf{n}_k \cdot [\rho_k (\mathbf{v}_k - \mathbf{v}^{int}) \psi_k + J_k] \right\} \quad (2.7)$$

where v_n^{int} is the normal component of velocity of the interface and Δt is the time interval of averaging. We should now make the appropriate choice of quantities \mathbf{J} , ϕ , and ψ in the averaged equation of general balance to obtain the equations of conservation of mass and momentum.

2.3.1 Conservation of Mass

The first assumption made here is that mass is transported by convection and diffusion term is equal to zero, therefore, we set $\psi_k = 1$, $\mathbf{J}_k = 0$, and $\phi_k = 0$ and the equation of conservation of mass for each phase is derived as follows [2]:

$$\frac{\partial(\bar{\rho}_k \alpha_k)}{\partial t} + \nabla \cdot (\bar{\rho}_k \alpha_k \widehat{\mathbf{v}}_k) = I_k \quad (2.8)$$

If we assume that there is not any mass transport between the phases through the interface ($I_k = 0$), and drop the overbars and overhats for the averaged values for sake of brevity, we have:

$$\boxed{\frac{\partial(\rho_k \alpha_k)}{\partial t} + \nabla \cdot (\rho_k \alpha_k \mathbf{v}_k) = 0} \quad (2.9)$$

2.3.2 Conservation of Momentum

The macroscopic the equation of conservation of momentum can be derived by setting $\psi_k = \mathbf{v}_k$, $J_k = -\boldsymbol{\pi}_k = p_k \boldsymbol{\delta} - \boldsymbol{\tau}_k$, and $\phi_k = \mathbf{g}_k$ which gives us the general momentum balance equation :

$$\frac{\partial(\alpha_k \bar{\rho}_k \hat{\mathbf{v}}_k)}{\partial t} + \nabla \cdot (\alpha_k \bar{\rho}_k \hat{\mathbf{v}}_k \hat{\mathbf{v}}_k) = -\nabla (\alpha_k \bar{p}_k) + \nabla \cdot [\alpha_k (\bar{\boldsymbol{\tau}}_k + \boldsymbol{\tau}_k^T)] + \alpha_k \bar{\rho}_k \mathbf{g} + M_k \quad (2.10)$$

and,

$$\mathbf{M}_k \equiv I_k = -\frac{1}{\Delta t} \sum_j \left\{ \frac{1}{v_{ni}} \mathbf{n}_k \cdot [\rho_k (\mathbf{v}_k - \mathbf{v}_i) \mathbf{v}_k - \boldsymbol{\pi}_k] \right\} \quad (2.11)$$

Where $\boldsymbol{\tau}_k^T$ is the fluctuations in the shear stress term (Turbulent stress). Equation 4.7 is expressed in terms of local instant variables, and therefore, it is not possible to use it in Equation 2.10. Hence, we need to formulate that in terms of averaged quantities. It is worth mentioning that when time or volume averaging is applied, not all characteristics of local two-phase flow can be brought into the averaged model.

Based on that, the surface area concentration per unit volume is defined as follows [1]:

$$a_{ij} \equiv \frac{1}{L_j} = \frac{1}{\Delta t} \lim_{\delta \rightarrow 0} \frac{2\varepsilon_j}{\delta} = \frac{1}{\Delta t} \left(\frac{1}{v_{ni}} \right)_j \quad (2.12)$$

Here δ is the interfacial thickness, $2\varepsilon_j = \delta/v_{ni}$ is the time interval associated with each interface, and index j is indicating each interface (bubble). Using Equation 2.12 and the interfacial mass flux, $\dot{m}_k \equiv \rho_k \mathbf{n}_k \cdot (\mathbf{v}_k - \mathbf{v}_i)$, we have:

$$\mathbf{M}_k = -\sum_j a_{ij} (\dot{m}_k \mathbf{v}_k + p_k \mathbf{n}_k - \mathbf{n}_k \cdot \boldsymbol{\tau}_k) \quad (2.13)$$

where the term inside bracket is rate of interfacial momentum loss per unit area for phase k. Using the definition of surface mean values which is given by:

$$\overline{\overline{F}}_{(i)} \equiv \left(\sum_j \frac{F}{L_j} \right) L_S = \frac{\sum_j a_{ij} F}{a_i} \quad (2.14)$$

Equation 2.13 can be written down in terms of the surface mean values:

$$\mathbf{M}_k = \mathbf{M}_k^I + \mathbf{M}_k^n + \overline{\overline{p}}_k^{int} \nabla \alpha_k + \mathbf{M}_k^t - \nabla \alpha_k \cdot \overline{\overline{\boldsymbol{\tau}}}_{ki} \quad (2.15)$$

where:

$$\begin{aligned} \mathbf{M}_k^I &= I_k \widehat{\mathbf{v}}_k^{int} \\ \mathbf{M}_k^n &\doteq \sum_j a_{ij} \left(\overline{\overline{p}}_k^{int} - p_k \right) \mathbf{n}_k \\ \mathbf{M}_k^t &\doteq \sum_j a_{ij} \mathbf{n}_k \cdot \left(\boldsymbol{\tau}_k - \overline{\overline{\boldsymbol{\tau}}}_k^{int} \right) \end{aligned} \quad (2.16)$$

Here, I_k represents the rate of mass transfer between the phases, and \mathbf{M}_k^n represents the form drag which is the drag force created due to the shape of the object and area of cross-section and lift force arising from the pressure imbalance at the interface. \mathbf{M}_k^t represents the skin drag due to the imbalance of shear forces caused by interactions between fluid and the skin of the object. With more simplification, the final form of interphase momentum transfer term can be derived as follows [2]:

$$\mathbf{M}_k = \overline{\overline{p}}_k^{int} \nabla \alpha_k + \mathbf{M}_{ik} - \nabla \alpha_k \cdot \overline{\overline{\boldsymbol{\tau}}}_k^{int} \quad (2.17)$$

Where $\mathbf{M}_{ik} = \mathbf{M}_k^t + \mathbf{M}_k^n$ is the total generalized drag force that accounts for the drag, lift, and skin drag force. Substituting it in the averaged equation of conservation of momentum, the following equation will be obtained:

$$\begin{aligned} \frac{\partial}{\partial t} (\alpha_k \overline{\overline{\rho}}_k \widehat{\mathbf{v}}_k) + \nabla \cdot (\alpha_k \overline{\overline{\rho}}_k \widehat{\mathbf{v}}_k \widehat{\mathbf{v}}_k) &= -\nabla \cdot (\alpha_k \overline{\overline{p}}_k^{int}) + \nabla \cdot [\alpha_k (\overline{\overline{\boldsymbol{\tau}}}_k + \boldsymbol{\tau}_k^T)] \\ &+ \alpha_k \overline{\overline{\rho}}_k \widehat{\mathbf{g}}_k + (\overline{\overline{p}}_k^{int} \nabla \alpha_k + \mathbf{M}_{ik} - \nabla \alpha_k \cdot \overline{\overline{\boldsymbol{\tau}}}_k^{int}) \end{aligned} \quad (2.18)$$

Dropping the overbars and overhats for the phase and mass averaged variables and turbulent contributions (since our focus is on laminar flow) and neglecting the mass transfer between the phases will result in:

$$\boxed{\frac{\partial}{\partial t} (\alpha_k \rho_k \mathbf{v}_k) + \nabla \cdot (\alpha_k \rho_k \mathbf{v}_k \mathbf{v}_k) = -\alpha_k \nabla p_k + \nabla \cdot (\alpha_k \boldsymbol{\tau}_k) + \alpha_k \rho_k \mathbf{g}_k + (p_k^{int} - p_k) \nabla \alpha_k + \mathbf{M}_{ik} - \nabla \alpha_k \cdot \boldsymbol{\tau}_k^{int}} \quad (2.19)$$

This is the final canonical form of conservation of momentum, assuming no mass transfer between the phases. We can simplify the above equation further for the dispersed flow of gas-liquid two-phase flow using several assumptions. If we neglect the surface tension effects in the dispersed flow regime, the interfacial pressure and shear stress of the continuous and dispersed phases would be equal:

$$p_c^{int} \approx p_d^{int} = p^{int} \quad (2.20)$$

Furthermore, the pressure of the dispersed phase would be approximately equal to the pressure at the interface since dispersed phase particles are very small and density is low:

$$p_d \approx p^{int} \quad (2.21)$$

The other simplifying assumption reasonable for the dispersed flow regime is that the interfacial shear stress, would be negligible:

$$\boldsymbol{\tau}_k^{int} \approx 0 \quad (2.22)$$

Using this assumptions, the conservation of momentum equations for each phase can be simplified further and the following equations will be obtained for the continuous and dispersed phase respectively [23]:

$$\frac{\partial}{\partial t} (\alpha_c \rho_c \mathbf{v}_c) + \nabla \cdot (\alpha_c \rho_c \mathbf{v}_c \mathbf{v}_c) = -\alpha_c \nabla p_c + \nabla \cdot (\alpha_c \boldsymbol{\tau}_c) + \alpha_c \rho_c \mathbf{g} + (p_c^{int} - p_c) \nabla \alpha_c + \mathbf{M}_{ik} \quad (2.23)$$

$$\frac{\partial}{\partial t} (\alpha_d \rho_d \mathbf{v}_d) + \nabla \cdot (\alpha_d \rho_d \mathbf{v}_d \mathbf{v}_d) = -\alpha_d \nabla p^{int} + \nabla \cdot (\alpha_d \boldsymbol{\tau}_d) + \alpha_d \rho_d \mathbf{g} + \mathbf{M}_{ik} \quad (2.24)$$

2.4 Derivation of the two-fluid model using volume averaging

In this section, we will go through the derivation of the model using volume averaging. Volume averaging can be considered as a mathematical technique that can transform local field variables to averaged field variables that are not dependent on local variables such as the size or velocity of each individual particle [6]

Volume averaging has been used to derive the two-fluid model most commonly using a phase indicator function [25]. However, another ad hoc approach to derive two-fluid model using volume averaging is the cell averaging method [6] which results in derivation of dispersion term in both conservation of mass and momentum equation. In this section, we will review and discuss these approaches for deriving the two-fluid model.

2.4.1 Derivation using a phase indicator function

Using a phase indicator function to derive a volume-averaged two-fluid model is the common approach in the literature. In this section, we explain and discuss the derivation by Yeoh et al. [25]. Volume average of quantity ϕ is defined as:

$$\langle \phi \rangle_V(t) = \lim_{V \rightarrow \infty} \frac{1}{V} \int \phi(x, y, z, t) dV \quad (2.25)$$

Where V is the volume based on averaging length scale. The phase indicator function $\mathcal{F}(x, y, z, t)$ of each phase is defined such that it would be equal to 1 when the phase is present and 0 otherwise:

$$\mathcal{F}_k(x, y, z, t) = \begin{cases} 1 & \text{if } (x, y, z) \text{ is within phase } k \text{ at time } t \\ 0 & \text{otherwise} \end{cases} \quad (2.26)$$

It can be shown that by applying volume averaging operator to the phase indicator function, volume fraction which basically shows the fraction of space occupied by each phase is obtained:

$$\langle \mathcal{F}_k \rangle = \lim_{V \rightarrow \infty} \frac{1}{V} \int \mathcal{F}_k(x, y, z, t) dV = \frac{V_k}{V} = \alpha_k \quad (2.27)$$

In order to find the averaged conservation equations, the equations of conservation of mass and momentum for single-phase flows will be multiplied by the phase indicator function and then the averaging operator is applied to the equations. In the procedure of deriving the averaged equation, the following properties of volume averaging will be used [25]:

$$\begin{aligned}\langle\langle a \rangle\rangle &= \langle a \rangle \\ \langle a + b \rangle &= \langle a \rangle + \langle b \rangle \\ \langle\langle a \rangle b \rangle &= \langle a \rangle \langle b \rangle\end{aligned}\tag{2.28}$$

and,

$$\left\langle \frac{\partial a}{\partial t} \right\rangle = \frac{\partial \langle a \rangle}{\partial t} \quad \text{Leibniz rule}\tag{2.29}$$

$$\left\langle \frac{\partial a}{\partial x_j} \right\rangle = \frac{\partial \langle a \rangle}{\partial x_j} = \nabla \langle a \rangle \quad \text{Gauss rule}\tag{2.30}$$

Conservation of mass

Multiplying the phase indicator function with the equation of conservation of mass for single-phase flow, we have:

$$\mathcal{F}_k \frac{\partial \rho_k}{\partial t} + \mathcal{F}_k \nabla \cdot (\rho_k \mathbf{v}_k) = 0\tag{2.31}$$

Drew and Passman [26] showed that the topological equation reflecting the material derivative of phase indicator function at the interface is equal to zero:

$$\frac{D\mathcal{F}_k}{Dt} = \frac{\partial \mathcal{F}_k}{\partial t} + \mathbf{v}^{\text{int}} \cdot \nabla \mathcal{F}_k = 0\tag{2.32}$$

Using the two above equations and the product rule, the following equation can be obtained:

$$\frac{\partial (\mathcal{F}_k \rho_k)}{\partial t} + \nabla \cdot (\mathcal{F}_k \rho_k \mathbf{v}_k) = \rho_k (\mathbf{v}_k - \mathbf{v}^{\text{int}}) \cdot \nabla \mathcal{F}_k\tag{2.33}$$

By volume averaging this equation and using the properties mentioned above, the following equation can be derived:

$$\frac{\partial \langle \mathcal{F}_k \rho_k \rangle}{\partial t} + \nabla \cdot \langle \mathcal{F}_k \rho_k \mathbf{v}_k \rangle = \langle \rho_k (\mathbf{v}_k - \mathbf{v}^{\text{int}}) \cdot \nabla \mathcal{F}_k \rangle = I'_k \quad (2.34)$$

Which is the instantaneous volume-averaged equation of conservation of mass. The right-hand side represents the interfacial mass source term. In practical computations, it is preferred to resolve the random transient distribution of the instantaneous field ϕ with time. In order to do so, the instantaneous field can be decomposed into a steady motion $\bar{\phi}$ and fluctuating motion ϕ' :

$$\phi = \bar{\phi} + \phi' \quad (2.35)$$

Where the overbar denotes time averaging. By definition, the time averaged of the fluctuating motion is equal to zero:

$$\bar{\phi'} = \lim_{T \rightarrow \infty} \frac{1}{T} \int \phi' dt = 0 \quad (2.36)$$

In order to reduce the complexity of modeling additional terms for averaged fluctuation quantities, mass-weighted and phase-weighted averages are defined as follows respectively:

$$\overline{\langle \phi \rangle} = \frac{\overline{\langle \mathcal{F}_k \phi \rangle}}{\overline{\langle \mathcal{F}_k \rangle}} \quad (2.37)$$

and,

$$\overline{\langle \psi \rangle} = \frac{\overline{\langle \rho_k \psi \rangle}}{\overline{\langle \rho_k \rangle}} \quad (2.38)$$

Now, using the averaging properties, it can be shown that [25]:

$$\begin{aligned} \overline{\langle \mathcal{F}_k \phi \rangle} &= \overline{\langle \mathcal{F}_k \rangle \langle \phi \rangle} \\ \overline{\langle \rho_k \psi \rangle} &= \overline{\langle \rho_k \rangle \langle \psi \rangle} \end{aligned} \quad (2.39)$$

If we time-average the instantaneous volume-averaged equations, suitable forms of the conservation of mass and momentum can be derived in terms of phase-weighted variables and mass-weighted averages.

Using the two above equations, Equation 2.34, and the averaging properties, the effective equation of conservation of mass in terms of the local volume fraction is obtained:

$$\frac{\partial(\alpha_k \rho_k)}{\partial t} + \nabla \cdot (\alpha_k \rho_k \mathbf{v}_k) = I_k \quad (2.40)$$

In case of zero mass transfer between the phases, $I_k = 0$, we have:

$$\boxed{\frac{\partial(\alpha_k \rho_k)}{\partial t} + \nabla \cdot (\alpha_k \rho_k \mathbf{v}_k) = 0} \quad (2.41)$$

For sake of brevity, we dropped the parenthesis and overbar denoting volume, mass-weighted, and phase-weighted averaging.

Conservation of momentum

Similar to the derivation of the conservation of mass equation, to derive the equation of multiphase conservation of momentum equation, we start from the single-phase equation, then we multiply by phase indicator function, and finally apply averaging operator and use the averaging properties to derive the averaged equation.

$$\rho_k \frac{\partial \mathbf{v}_k}{\partial t} + \rho_k \mathbf{v}_k \cdot \nabla \mathbf{v}_k = -\nabla p_k + \nabla \cdot \boldsymbol{\tau}_k + \sum \mathbf{F}_{k, \text{ body forces}} \quad (2.42)$$

Where the body forces is gravitational force i.e. $\sum \mathbf{F}_{k, \text{ body forces}} = \rho_k \mathbf{g}$. If we multiply by the phase indicator function, we get:

$$\mathcal{F}_k \rho_k \frac{\partial \mathbf{v}_k}{\partial t} + \mathcal{F}_k \rho_k \mathbf{v}_k \cdot \nabla \mathbf{v}_k = -\mathcal{F}_k \nabla p_k + \mathcal{F}_k \nabla \cdot \boldsymbol{\tau}_k + \mathcal{F}_k \rho_k \mathbf{g} \quad (2.43)$$

Using Equation 2.33 and the product rule, for the first term on left-hand side, we have:

$$\mathcal{F}_k \rho_k \frac{\partial \mathbf{v}_k}{\partial t} = \frac{\partial(\mathcal{F}_k \rho_k \mathbf{v}_k)}{\partial t} + \mathbf{v}_k \cdot \nabla (\mathcal{F}_k \rho_k \mathbf{v}_k) - \rho_k \mathbf{v}_k (\mathbf{v}_k - v^{\text{int}}) \cdot \nabla \mathcal{F}_k \quad (2.44)$$

For the second term on right hand-side (advection term) we have:

$$\mathcal{F}_k \rho_k \mathbf{v}_k \cdot \nabla \mathbf{v}_k = \nabla \cdot (\mathcal{F}_k \rho_k \mathbf{v}_k \mathbf{v}_k) - \mathbf{v}_k \cdot \nabla (\mathcal{F}_k \rho_k \mathbf{v}_k) \quad (2.45)$$

Substituting the two above equations in Equation 2.43, we obtain:

$$\begin{aligned} \frac{\partial (\mathcal{F}_k \rho_k \mathbf{v}_k)}{\partial t} + \nabla \cdot (\mathcal{F}_k \rho_k \mathbf{v}_k \mathbf{v}_k) &= -\nabla (\mathcal{F}_k p_k) + \nabla \cdot (\mathcal{F}_k \boldsymbol{\tau}_k) \\ &+ p_k \nabla \mathcal{F}_k k \mathbf{v}_k (\mathbf{v}_k - v_{\text{int}}) \cdot \nabla \mathcal{F}_k - \boldsymbol{\tau}_k \cdot \nabla \mathcal{F}_k + \mathcal{F}_k \rho_k \mathbf{g} \end{aligned} \quad (2.46)$$

Applying volume averaging and using the properties, we get:

$$\begin{aligned} \frac{\partial \langle \mathcal{F}_k \rho_k \mathbf{v}_k \rangle}{\partial t} + \nabla \cdot \langle \mathcal{F}_k \rho_k \mathbf{v}_k \mathbf{v}_k \rangle &= -\nabla \langle \mathcal{F}_k p_k \rangle + \nabla \cdot \langle \mathcal{F}_k \boldsymbol{\tau}_k \rangle + \langle \mathcal{F}_k \rangle \langle \rho_k \mathbf{g} \rangle \\ &+ \underbrace{\langle \rho_k \mathbf{v}_k (\mathbf{v}_k - v_{\text{int}}) \cdot \nabla \mathcal{F}_k \rangle + \langle p_k \rangle \langle \nabla \mathcal{F}_k \rangle - \langle \boldsymbol{\tau}_k \cdot \nabla \mathcal{F}_k \rangle}_{\mathbf{M}_k} \end{aligned} \quad (2.47)$$

Where the term \mathbf{M}_k is the interphase momentum source term. Similar to what we did in the previous section, we use phase-weighted and mass-weighted average to formulate the effective equation of conservation of momentum which includes local volume fraction:

$$\begin{aligned} \frac{\partial (\alpha_k \rho_k \mathbf{v}_k)}{\partial t} + \nabla \cdot (\alpha_k \rho_k \mathbf{v}_k \mathbf{v}_k) &= -\alpha_k \nabla p_k - p_k \nabla \alpha_k + \nabla \cdot (\alpha_k \boldsymbol{\tau}_k) - \nabla \cdot (\alpha_k \boldsymbol{\tau}_k^T) \\ &+ \alpha_k \rho_k \mathbf{g} + \mathbf{M}_k \end{aligned} \quad (2.48)$$

and,

$$\mathbf{M}_k = \sum_{l=1}^N (\dot{m}_{lk} \mathbf{v}_l - \dot{m}_{kl} \mathbf{v}_k) + p_k^{\text{int}} \nabla \alpha_k + \mathbf{F}_k^{\text{D}} \quad (2.49)$$

Where the interfacial force, \mathbf{F}_k^{D} , can be split in terms of drag and non-drag forces and \dot{m}_{lk} and \dot{m}_{kl} characterize the mass transfer from phase l to phase k and from phase k to phase l, respectively. Now, by substituting Equation 2.49 in Equation 2.48, we get:

$$\begin{aligned}
\frac{\partial(\alpha_k \rho_k \mathbf{v}_k)}{\partial t} + \nabla \cdot (\alpha_k \rho_k \mathbf{v}_k \mathbf{v}_k) &= -\alpha_k \nabla p_k - p_k \nabla \alpha_k + \nabla \cdot (\alpha_k \boldsymbol{\tau}_k) - \nabla \cdot (\alpha_k \boldsymbol{\tau}_k^T) \\
&+ \alpha_k \rho_k \mathbf{g} + \sum_{l=1}^N (\dot{m}_{lk} \mathbf{v}_l - \dot{m}_{kl} \mathbf{v}_k) + p_k^{\text{int}} \nabla \alpha_k + \mathbf{F}_k^{\text{D}}
\end{aligned} \tag{2.50}$$

Assuming that the mass transfer between the phases is zero and neglecting the turbulent contributions, we obtain the final canonical form of conservation of momentum:

$$\boxed{
\begin{aligned}
\frac{\partial(\alpha_k \rho_k \mathbf{v}_k)}{\partial t} + \nabla \cdot (\alpha_k \rho_k \mathbf{v}_k \mathbf{v}_k) &= -\alpha_k \nabla p_k - p_k \nabla \alpha_k + \nabla \cdot (\alpha_k \boldsymbol{\tau}_k) \\
&+ \alpha_k \rho_k \mathbf{g} + p_k^{\text{int}} \nabla \alpha_k + \mathbf{F}_k^{\text{D}}
\end{aligned}
} \tag{2.51}$$

2.4.2 Derivation using cell averaging method

In this section, the derivation of the two-fluid model for inviscid bubbly flow by Espinosa-Paredes et al. [6] using volume averaging and cell averaging method will be reviewed. The main difference between this derivation and the previous section derivation is that the phase indicator function is not involved in this derivation.

In order to obtain the averaged field equations, an integral over averaging volume, \mathcal{V} , must be applied to each term of the local field equations. The averaging volume is constant, smaller than the size of the system, and also larger than the size of the bubbles and the separation distance between adjacent bubbles as shown in Figure 2.5 In order to obtain meaningful averaged quantities, the characteristic length of each phase should be greatly smaller than the characteristic length of averaging. In addition, the characteristic length of averaging should be smaller than the domain of the system:

$$\ell_k \ll r_o \ll L \tag{2.52}$$

The superficial volume average of some function ψ_k associated with the kth-phase is defined as:

$$\langle \psi_k \rangle (\mathbf{x}, t) = \frac{1}{\mathcal{V}} \int_{V_k(\mathbf{x}, t)} \psi_k (\mathbf{x} + \mathbf{y}_k, t) dV_y \tag{2.53}$$

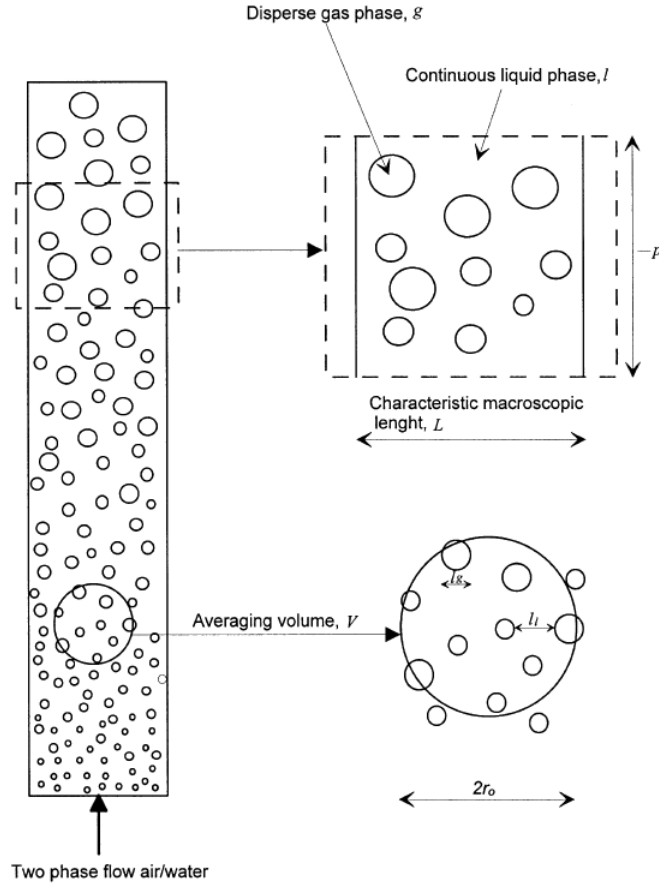


Figure 2.5: The scale of the system, characteristic lengths, and averaging volume of each phase [6]

where $V_k(\mathbf{x}, t)$ is the volume of the k th-phase contained within the averaging volume \mathcal{V} which is independent of space and time. For sake of simplicity the superficial average of ψ_k can be written as:

$$\langle \psi_k \rangle = \frac{1}{\mathcal{V}} \int_{V_k} \psi_k \, dV \quad (2.54)$$

The intrinsic average which is defined over the volume of phase k instead of the averaging volume is expressed in form of:

$$\langle \psi_k \rangle^k = \frac{1}{V_k} \int_{V_k} \psi_k \, dV \quad (2.55)$$

Dividing the two above equations, knowing that $V_k/\mathcal{V} = \alpha_k$, the following correlation between the average over each phase and the superficial average can be obtained:

$$\langle \psi_k \rangle = \alpha_k \langle \psi_k \rangle^k \quad (2.56)$$

In order to obtain the volume-averaged equation of conservation of mass and momentum, we need to use two averaging theorems. The first one is the transport theorem [27, 28]:

$$\left\langle \frac{\partial \psi_k}{\partial t} \right\rangle = \frac{\partial \langle \psi_k \rangle}{\partial t} - \frac{1}{\mathcal{V}} \int_{A^{int}(t)} \psi_k \mathbf{v}^{int} \cdot \mathbf{n}^{int} \, dA \quad (2.57)$$

The second integral theorem is the spatial averaging theorem [27, 29]:

$$\langle \nabla \psi_k \rangle = \nabla \langle \psi_k \rangle + \frac{1}{\mathcal{V}} \int_{A^{int}(t)} \psi_k \mathbf{n}^{int} \, dA \quad (2.58)$$

Where A^{int} is the interfacial area. Now, we can derive the volume-averaged equation of conservation of mass:

$$\left\langle \frac{\partial \rho_k}{\partial t} \right\rangle + \langle \nabla \cdot (\rho_k \mathbf{v}_k) \rangle = 0 \quad (2.59)$$

Using the two above theorems shown in Equations 2.57 and 2.58, Equation 2.59 can be written as:

$$\frac{\partial \langle \rho_k \rangle}{\partial t} + \nabla \cdot \langle \rho_k \mathbf{v}_k \rangle + \frac{1}{\mathcal{V}} \int_{A^{int}(t)} \rho_k (\mathbf{v}_k - \mathbf{v}^{int}) \cdot \mathbf{n}^{int} \, dA = 0 \quad (2.60)$$

Assuming that the interfacial mass transfer is zero, the fluid velocity in each phase is equal to the velocity of interface. Therefore, the third term of the equation will be zero and the above equation simplifies to:

$$\frac{\partial \langle \rho_k \rangle}{\partial t} + \nabla \cdot \langle \rho_k \mathbf{v}_k \rangle = 0 \quad (2.61)$$

where averaged quantities are defined as:

$$\begin{aligned}\mathbf{v}_k &= \langle \mathbf{v}_k \rangle^k + \tilde{\mathbf{v}}_k \\ \rho_k &= \langle \rho_k \rangle^k + \tilde{\rho}_k\end{aligned}\tag{2.62}$$

where $\tilde{\mathbf{v}}_k$ and $\tilde{\rho}_k$ are the spatial deviations of the velocity and density, respectively.

Considering the averaging quantities, we have:

$$\langle \rho_k \mathbf{v}_k \rangle = \alpha_k \langle \rho_k \mathbf{v}_k \rangle^k = \alpha_k \langle \rho_k \rangle^k \langle \mathbf{v}_k \rangle^k + \alpha_k \langle \tilde{\rho}_k \tilde{\mathbf{v}}_k \rangle^k\tag{2.63}$$

By substituting the above equation in Equation 2.61, the following equation will be obtained:

$$\frac{\partial \alpha_k \langle \rho_k \rangle^k}{\partial t} + \nabla \cdot \left(\alpha_k \langle \rho_k \rangle^k \langle \mathbf{v}_k \rangle^k \right) + \nabla \cdot \left(\alpha_k \langle \tilde{\rho}_k \tilde{\mathbf{v}}_k \rangle^k \right) = 0\tag{2.64}$$

where the third term shows the dispersion of mass caused by deviations in the velocity. For many flows in which thermal and pressure gradients are not very large, the term including the spatial deviation of density ($\tilde{\rho}_k$) would be very small, and hence, the dispersion term could be neglected. It will also be proved using scaling analysis in the next chapter. Therefore the final form of conservation of mass will be:

$$\frac{\partial \alpha_k \langle \rho_k \rangle^k}{\partial t} + \nabla \cdot \left(\alpha_k \langle \rho_k \rangle^k \langle \mathbf{v}_k \rangle^k \right) = 0\tag{2.65}$$

dropping the angled brackets for phasic averaged quantities for brevity, the conservation of mass equation can be written as:

$$\boxed{\frac{\partial (\alpha_k \rho_k)}{\partial t} + \nabla \cdot (\alpha_k \rho_k \mathbf{v}_k) = 0}\tag{2.66}$$

Similarly, the averaged equation of conservation of momentum can be derived by applying the volume averaging operator on the single-phase equation:

$$\left\langle \frac{\partial (\rho_k \mathbf{v}_k)}{\partial t} \right\rangle + \langle \nabla \cdot (\rho_k \mathbf{v}_k \mathbf{v}_k) \rangle + \langle \nabla \cdot (p_k \delta_{ij}) \rangle - \langle \nabla \cdot \boldsymbol{\tau}_k \rangle - \langle \rho_k \mathbf{g}_k \rangle = 0\tag{2.67}$$

which after using the averaging properties and the two theorems presented in Equations 2.57 and 2.58, it will simplify to the form:

$$\begin{aligned} \frac{\partial}{\partial t} \left(\alpha_k \langle \rho_k \rangle^k \langle \mathbf{v}_k \rangle^k \right) + \nabla \cdot \left(\alpha_k \langle \rho_k \rangle^k \langle \mathbf{v}_k \rangle^k \langle \mathbf{v}_k \rangle^k \right) + \alpha_k \nabla \langle p_k \rangle^k - \alpha_k \langle \rho_k \rangle^k \mathbf{g} \\ = \langle \Delta p^{int} \rangle \nabla \alpha_k - \nabla \cdot \left(\alpha_k \langle \rho_k \rangle^k \langle \tilde{\mathbf{v}}_k \tilde{\mathbf{v}}_k \rangle^k \right) + \mathbf{M}^{int} \end{aligned} \quad (2.68)$$

where the second term on the right-hand side represents the dispersion of momentum.

The averaged pressure difference over the interface can be calculated from Equation 2.55 and it is equal to [6]:

$$\langle \Delta p^{int} \rangle \nabla \alpha_k = -\frac{1}{\mathcal{V}} \int_{A^{int}(t)} \mathbf{n}^{int} \langle \Delta p^{int} \rangle dA = -\langle \Delta p^{int} \rangle \left(\frac{1}{\mathcal{V}} \int_{A^{int}(t)} \mathbf{n}^{int} dA \right) \quad (2.69)$$

The same applies to other terms on the right-hand side. However, it is not practical to use these correlations in the macroscopic (hydrodynamic) equations, and as a results, closure terms need to be used to close the equations of conservation of momentum for the pressure difference, dispersion, and interphase momentum exchange terms. Therefore, the canonical form of the equation of conservation momentum (without closure) is obtained as follows:

$$\boxed{\frac{\partial}{\partial t} (\alpha_k \rho_k \mathbf{v}_k) + \nabla \cdot (\alpha_k \rho_k \mathbf{v}_k \mathbf{v}_k) = -\alpha_k \nabla p_k + \alpha_k \rho_k \mathbf{g} + \langle \Delta p^{int} \rangle \nabla \alpha_k - \nabla \cdot (\alpha_k \rho_k \langle \tilde{\mathbf{v}}_k \tilde{\mathbf{v}}_k \rangle) + \mathbf{M}'_k} \quad (2.70)$$

where the last three terms need to be defined using closures to close the equation of conservation of momentum.

2.5 Derivation of the two-fluid model using kinetic theory of gases and ensemble averaging

In this section, another approach for the derivation of the dispersed phase conservation equations using the kinetic theory will be reviewed and discussed for the case of inviscid dispersed phase with no collision between the particles based on Gidaspow's derivation [20].

2.5.1 Kinetic theory principles

In order to use kinetic theory for the derivation of conservation equations, first, we will introduce some basic principles and correlation.

The frequency distribution of the velocity of particles, f , is a function of time t , position \mathbf{x} , and instantaneous (microscopic) velocity \mathbf{c} which basically represents the number of particles per unit volume at a given time, position, and velocity [20].

$$f = f(t, \mathbf{x}, \mathbf{c}) \quad (2.71)$$

The number of particles per unit volume, n (number density) can be calculated by integrating over the frequency distribution function:

$$n = \int f(t, \mathbf{x}, \mathbf{c}) d\mathbf{c} \quad (2.72)$$

The mean statistical or ensemble average of quantity ϕ can be calculated as follows:

$$n \langle \phi \rangle = \int \phi f(t, \mathbf{x}, \mathbf{c}) d\mathbf{c} \quad (2.73)$$

Therefore, the hydrodynamic or macroscopic velocity will be

$$\mathbf{v} = \frac{1}{n} \int \mathbf{c} f(t, \mathbf{x}, \mathbf{c}) d\mathbf{c} \quad (2.74)$$

2.5.2 Boltzmann Transport Equation

The Boltzmann equation or Boltzmann transport equation describes the behaviour of a system when it is not in a state of equilibrium, for the frequency distribution function, f , it is given as follows:

$$\frac{\partial f}{\partial t} + \mathbf{c} \cdot \frac{\partial f}{\partial \mathbf{x}} + \mathbf{F} \frac{\partial f}{\partial \mathbf{c}} = \left(\frac{\partial f}{\partial t} \right)_{coll} \quad (2.75)$$

where $\mathbf{F} = \frac{d\mathbf{c}}{dt}$ is the force per unit mass or the instantaneous acceleration and $\left(\frac{\partial f}{\partial t} \right)_{coll}$ shows the rate of change of collision between particles with time.

Chapman and Cowling [30] introduced a relative velocity in terms of hydrodynamic velocity:

$$\mathbf{C} = \mathbf{c} - \mathbf{v}(t, \mathbf{x}) \quad (2.76)$$

Which basically changes the coordinate from \mathbf{c} to \mathbf{C} :

$$f(t, \mathbf{x}, \mathbf{c}) = f_c(t, \mathbf{x}, \mathbf{C}) \quad (2.77)$$

Multiplying the Boltzmann Equation by \mathbf{C} and using the chain rule, the modified Boltzmann Equation with respect to material derivative can be derived:

$$\frac{Df}{Dt} + \mathbf{C} \frac{\partial f}{\partial \mathbf{x}} + \left(\mathbf{F} - \frac{D\mathbf{v}}{Dt} \right) \frac{\partial f}{\partial \mathbf{C}} - \frac{\partial f}{\partial \mathbf{C}} \mathbf{C} : \frac{\partial \mathbf{v}}{\partial \mathbf{x}} = \left(\frac{\partial f}{\partial t} \right)_{\text{coll}} \quad (2.78)$$

2.5.3 Maxwell Transport Equation

The transport equation for a quantity ψ can be derived by multiplying Boltzmann Transport Equation by ψ and integrating over the instantaneous velocity \mathbf{c} [20]:

$$\int \psi \left(\frac{\partial f}{\partial t} + \mathbf{c} \cdot \frac{\partial f}{\partial \mathbf{x}} + \mathbf{F} \cdot \frac{\partial f}{\partial \mathbf{c}} \right) d\mathbf{c} = \int \psi \left(\frac{\partial f}{\partial t} \right)_{\text{coll}} d\mathbf{c} \quad (2.79)$$

We can transform these integrals using the following correlation [20]:

$$\begin{aligned} \int \psi \frac{\partial f}{\partial t} d\mathbf{c} &= \frac{\partial}{\partial t} \int \psi f d\mathbf{c} - \int f \frac{\partial \psi}{\partial t} d\mathbf{c} = \frac{\partial n \langle \psi \rangle}{\partial t} - n \langle \frac{\partial \psi}{\partial t} \rangle \\ \int \psi c_x \frac{\partial f}{\partial x} d\mathbf{c} &= \frac{\partial}{\partial x} \int \psi c_x f d\mathbf{c} - \int f c_x \frac{\partial \psi}{\partial x} d\mathbf{c} = \frac{\partial n \langle \psi c_x \rangle}{\partial x} - n \langle c_x \frac{\partial \psi}{\partial x} \rangle \\ \int \psi \frac{\partial f}{\partial c_x} d\mathbf{c} &= \iint [\psi f]_{c_x=-\infty}^{c_x=\infty} dc_y dc_x - \int f \frac{\partial \psi}{\partial c_x} d\mathbf{c} = -n \langle \frac{\partial \psi}{\partial c_x} \rangle \end{aligned} \quad (2.80)$$

Using the above equations, we can simplify the Maxwell Transport Equation as follows:

$$\frac{\partial n \langle \psi \rangle}{\partial t} + \frac{\partial}{\partial \mathbf{x}} \cdot n \langle \psi \mathbf{c} \rangle - n \left[\langle \frac{\partial \psi}{\partial t} \rangle + \langle \mathbf{c} \cdot \frac{\partial \psi}{\partial \mathbf{x}} \rangle + \mathbf{F} \cdot \langle \frac{\partial \psi}{\partial \mathbf{c}} \rangle \right] = \int \psi \left(\frac{\partial f}{\partial t} \right)_{\text{coll}} d\mathbf{c} \quad (2.81)$$

This equation can be written in a more convenient form for derivation of conservation equations if we change the coordinates to the relative velocity (\mathbf{C}) and write it for the quantity $\psi = \psi\langle C \rangle$ using the chain rule [20]:

$$\frac{Dn\langle\psi\rangle}{Dt} + n\langle\psi\rangle\frac{\partial\mathbf{v}}{\partial\mathbf{x}} + \frac{\partial}{\partial\mathbf{x}}n\langle\psi\mathbf{C}\rangle - n\left(\mathbf{F} - \frac{D\mathbf{v}}{Dt}\right)\langle\frac{\partial\psi}{\partial\mathbf{C}}\rangle - n\langle\frac{\partial\psi}{\partial\mathbf{C}}\mathbf{C}\rangle : \frac{\partial\mathbf{v}}{\partial\mathbf{x}} = n\psi_c \quad (2.82)$$

This equation can be used to derive the conservation of mass and momentum equations without considering collisions by substituting appropriate quantity for ψ .

Conservation of mass

To derive the conservation of mass equation, we need to substitute $\psi = m$ in Equation 2.82, and by this substitution, all the terms except for the first two will cancel out and the following equation will be obtained [20]:

$$\frac{D(nm)}{Dt} + nm\frac{\partial\mathbf{v}}{\partial\mathbf{x}} = 0 \quad (2.83)$$

Knowing that the bulk density, ρ , is equal to $\rho = nm = \rho_d\alpha_d$ we can simplify to get [20]:

$$\frac{\partial(\alpha_d\rho_d)}{\partial t} + \frac{\partial(\alpha_d\rho_d\mathbf{v}_d)}{\partial\mathbf{x}} = 0 \quad (2.84)$$

Using the nabla operator, the equation of conservation of mass for dispersed phase will be obtained as follows:

$$\boxed{\frac{\partial(\alpha_d\rho_d)}{\partial t} + \nabla\cdot(\alpha_d\rho_d\mathbf{v}_d) = 0} \quad (2.85)$$

Conservation of momentum

In order to derive the conservation of momentum equation, let $\psi = mC$ in Equation 2.82. The average relative velocity of the particles will to be zero, taking into account the definition of \mathbf{v} :

$$\langle \mathbf{C} \rangle = \langle \mathbf{c} \rangle - \mathbf{v} = 0 \quad (2.86)$$

As a result, the first two terms in Equation 2.82 zero out, and for the rest, we have:

$$\frac{\partial}{\partial \mathbf{x}} nm \langle \mathbf{C}\mathbf{C} \rangle - n \left(\mathbf{F} - \frac{D\mathbf{v}}{Dt} \right) \langle m \frac{\partial \mathbf{C}}{\partial \mathbf{C}} \rangle - nm \langle \mathbf{C} \rangle : \frac{\partial \mathbf{v}}{\partial \mathbf{x}} = 0 \quad (2.87)$$

The last term on the right hand side would also zero out since it is being multiplied by $\langle \mathbf{C} \rangle = 0$:

$$\frac{\partial}{\partial \mathbf{x}} nm \langle \mathbf{C}\mathbf{C} \rangle - nm \left(\mathbf{F} - \frac{D\mathbf{v}}{Dt} \right) = 0 \quad (2.88)$$

With more simplifications, we have:

$$\frac{\partial}{\partial \mathbf{x}} \rho \langle \mathbf{C}\mathbf{C} \rangle - \rho \left(\mathbf{F} - \frac{D\mathbf{v}}{Dt} \right) = 0 \quad (2.89)$$

Which is the inviscid momentum balance equation of the dispersed phase.

The tensor $\rho \langle \mathbf{C}\mathbf{C} \rangle$ is defined as kinetic part of the stress:

$$\mathbf{P}_k = \rho \langle \mathbf{C}\mathbf{C} \rangle \quad (2.90)$$

If we write it in the matrix form, we get:

$$\mathbf{P}_k \equiv \rho \langle \mathbf{C}\mathbf{C} \rangle = \begin{bmatrix} \rho \langle C_x^2 \rangle & \rho \langle C_x C_y \rangle & \rho \langle C_x C_z \rangle \\ \rho \langle C_y C_x \rangle & \rho \langle C_y^2 \rangle & \rho \langle C_y C_z \rangle \\ \rho \langle C_z C_x \rangle & \rho \langle C_z C_y \rangle & \rho \langle C_z^2 \rangle \end{bmatrix} \quad (2.91)$$

Therefore the final form of momentum equation will be [20]:

$$\frac{\partial}{\partial \mathbf{x}} \mathbf{P}_k - \rho \left(\mathbf{F} - \frac{D\mathbf{v}}{Dt} \right) = 0 \quad (2.92)$$

If we write it in conservative form using the nabla operator, we get:

$$\boxed{\frac{\partial (\alpha_d \rho_d \mathbf{v}_d)}{\partial t} + \nabla \cdot (\alpha_d \rho_d \mathbf{v}_d \mathbf{v}_d) = -\nabla \cdot \mathbf{P}_k + \alpha_d \rho_d \mathbf{F}} \quad (2.93)$$

2.6 Derivation of the two-fluid model using a modified control volume

This section introduces and explains a less studied approach originally from Brennen [21] to derive the two-fluid model. In this derivation, the control volume will be modified which results in the derivation of a different momentum equation for the dispersed phase.

In this derivation, a control volume of dimensions ϵ assuming that ϵ is much smaller than the typical distances over which flow properties vary significantly is used. It is assumed that ϵ is much larger than the size of dispersed phase particles. The first assumption is required to define the derivative of flow properties in the flow field. The second assumption is necessary so that each averaging volume contains enough samples of each phase to represent the entire flow [21].

Choosing this control volume with the properties mentioned above is one of the challenges in studying multiphase flow. Generally, the properties of each phase, especially the continuous phase, vary significantly within the control volume, which brings about challenges of defining averaging quantities [21]. Additionally, the intersection of dispersed phase particles with the boundary of the control volume can give rise to non-physicality in the resulting conservation equations. Hence, extra care will be taken in this derivation with the control volume.

2.6.1 Conservation of mass

In order to derive the conservation of mass for dispersed multiphase flow, a cubic control volume is adopted. The mass flow rate of each phase is given by $\rho_k j_{ki}$, where $j_{ki} = \alpha_k \mathbf{v}_{ki}$ and k and i show each phase and direction respectively. The net rate of outflow of mass from the control volume is calculated by the divergence of the mass flow rate:

$$\frac{\partial(\rho_k \alpha_k \mathbf{v}_{ki})}{\partial x_i} \tag{2.94}$$

The rate of accumulation of mass of each phase in the control volume is given by:

$$\frac{\partial(\rho_k \alpha_k)}{\partial t} \tag{2.95}$$

Therefore, the equation of conservation of mass for each phase is given by:

$$\frac{\partial(\rho_k \alpha_k)}{\partial t} + \frac{\partial(\rho_k \alpha_k \mathbf{v}_{ki})}{\partial x_i} = I_k \quad (2.96)$$

If we write it using nabla operator it will be:

$$\frac{\partial(\rho_k \alpha_k)}{\partial t} + \nabla \cdot (\rho_k \alpha_k \mathbf{v}_k) = I_k \quad (2.97)$$

Where I_k is the rate of mass transfer to phase k from other phases. It is worth mentioning that, in order for conservation of mass to hold, the net rate of mass transfer between the phases must be zero:

$$\sum_k I_k = 0 \quad (2.98)$$

2.6.2 Conservation of momentum

In this section, the equations of conservation of momentum are derived for the control volume. To avoid the difficulty of the presence of both phases at the boundary of the control volume, a minor modification is made on the control volume. It is slightly deformed so that it does not cut across the dispersed phase and instead only crosses the continuous phase. Figure 2.6 shows the modified control volume. Considering the microscopic dimensions of the dispersed phase particles compared to the control volume, this modification has only a small impact on the system. Yet, it avoids complications of determining volume fraction and the force imposed by each phase to the others when the control volume boundary intersects particles [21].

Now, using the conservation of momentum principles, the rate of change of momentum in the control volume by time is given by:

$$\frac{\partial(\rho_k \alpha_k \mathbf{v}_k)}{\partial t} \quad (2.99)$$

and the net flux of momentum out of the control volume is:

$$\frac{\partial(\rho_k \alpha_k \mathbf{v}_{ki} \mathbf{v}_k)}{\partial x_i} \quad (2.100)$$

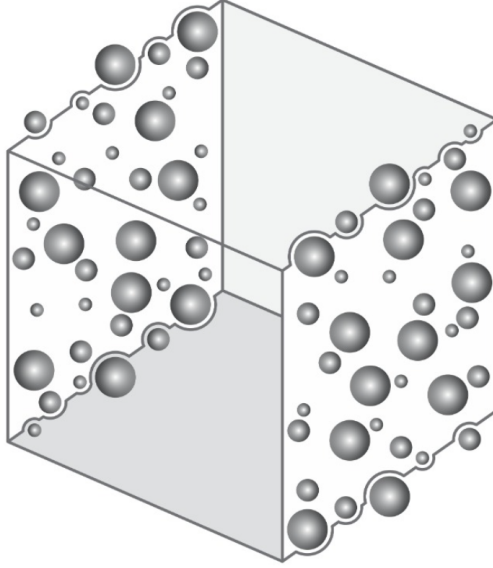


Figure 2.6: The modified control volume used in derivation of the momentum equations

The summation of these two contributions is equal to the net force acting on each phase in the control volume:

$$\mathbf{F}'_k = \frac{\partial(\rho_k \alpha_k \mathbf{v}_k)}{\partial t} + \frac{\partial(\rho_k \alpha_k \mathbf{v}_{ki} \mathbf{v}_k)}{\partial x_i} \quad (2.101)$$

To complete the equations of motion, the term \mathbf{F}'_k should be defined. It accounts for the total force per unit volume and includes body forces, forces due to pressure and stress, and the interfacial force acting within the control volume. Body force is exerted without requiring any contact, and forces due to gravity, magnetic, and electric fields are examples. However, in this work, only gravitational force is included. The other forces that should be included in the left-hand side of the above equation are the forces due to pressure and viscous stress, referred to as molecular fluxes. Finally, the third group of forces considered in each phase's conservation of momentum equation is the forces imposed by each phase to the others within the control volume [21].

As mentioned above, the body force we have here is the gravitational force, which is defined as:

$$\alpha_k \rho_k \mathbf{g} \quad (2.102)$$

The second contribution, the molecular flux of momentum through the control volume, will be different for the two phases assuming that the control volume is deformed and does not intersect with the dispersed phase particles. Since particles of the dispersed phase are not present at the boundary of the control volume, there would be no molecular flux of momentum in the dispersed phase equation. As a result, pressure and viscous stress term vanish in the conservation of momentum of the dispersed phase. For the continuous phase, the molecular flux of momentum is equal to:

$$\frac{\partial \boldsymbol{\pi}_{ci}}{\partial x_i} \quad (2.103)$$

where

$$\boldsymbol{\pi}_{ci} = -p\boldsymbol{\delta}_{ij} + \boldsymbol{\tau}_{ci} \quad (2.104)$$

and p , $\boldsymbol{\delta}_{ij}$, and $\boldsymbol{\tau}_c$ are the pressure of the continuous phase, the Kronecker delta, and the deviatoric stress tensor of the continuous phase.

The third contribution to \mathbf{F}'_k is the force imposed on phase k by the other phase within the control volume. It is referred to as \mathbf{M}_k here. Now, we can write the conservation of momentum equation for each phase:

$$\frac{\partial(\rho_k \alpha_k \mathbf{v}_k)}{\partial t} + \frac{\partial(\rho_k \alpha_k \mathbf{v}_{ki} \mathbf{v}_k)}{\partial x_i} = \alpha_k \rho_k \mathbf{g} + \boldsymbol{\delta}_{ck} \left[-\frac{\partial p}{\partial x_i} + \frac{\partial \boldsymbol{\tau}_{ci}}{\partial x_i} \right] + \mathbf{M}_k \quad (2.105)$$

where the Kronecker delta, $\boldsymbol{\delta}_{ck}$ would be non-zero only for the continuous phase (*i.e.* $k=c$). Similar to the mass transfer between the phases, the net exchange of momentum between the two phases is equal to zero:

$$\sum_k \mathbf{M}_k = 0 \quad (2.106)$$

As a result, for two-phase flow, we have:

$$\mathbf{M}_d = -\mathbf{M}_c \quad (2.107)$$

In dispersed multiphase flow, the momentum exchange term, \mathbf{M}_k is decomposed into two different contributions, one due to pressure gradient in the continuous phase, $\frac{\partial p}{\partial x_i}$, and

the remainder due to other interactions between the phases such as drag, virtual mass, etc. which are added to the model as closure terms, \mathbf{M}'_k . Therefore the term \mathbf{M}_k for each phase is defined as [21]:

$$\mathbf{M}_d = -\mathbf{M}_c = -\alpha_d \frac{\partial p}{\partial x_i} + \mathbf{M}'_d \quad (2.108)$$

The presence of the pressure term might not be intuitive at the first glance and need more clarification on how it is derived and included as a momentum exchange term. In order to explain the presence of this term as a momentum exchange term, we make the assumptions of uniform pressure gradient within the control volume. Consequently, the force on the dispersed phase particles in the control volume due to the pressure of continuous phase is given by:

$$\mathbf{F}_d^p = \sum_N \int_A \mathbf{n} \cdot (p \boldsymbol{\delta}_{ij}) dA \quad (2.109)$$

Where N is the number of particles in the control volume. To make the calculations easier, we assume that particles are cubic with the volume of $V_p = (\Delta x)^3$, area of each face $A_p = (\Delta x)^2$, and three pairs of surfaces in each direction (i). Hence, the force in each direction of the particle (cubic) would be equal to:

$$\mathbf{F}_d^p = \sum_i F_d^{ip} \boldsymbol{\delta}_i = \sum_N \sum_i \int_{A_i} \mathbf{n} \cdot (p \boldsymbol{\delta}_{ij}) dA_i = \sum_i n A_p (-p|_{x_i+\Delta x} + p|_{x_i}) \boldsymbol{\delta}_i \quad (2.110)$$

Now, we multiply and divide by Δx and sum over the total number of particles in the control volume (N) which are identical.

$$\mathbf{F}_d^p = N(\Delta x)^2 \sum_i (\Delta x) \frac{-p|_{x_i+\Delta x} + p|_{x_i}}{\Delta x} \boldsymbol{\delta}_i = N(\Delta x)^3 \sum_i \frac{-p|_{x_i+\Delta x} + p|_{x_i}}{\Delta x} \boldsymbol{\delta}_i \quad (2.111)$$

Since dimensions of the particles are infinitesimal compared to the control volume ($\Delta x \rightarrow 0$), we have:

$$\mathbf{F}_d^p = -NV_p \sum_i \frac{\partial p}{\partial x_i} \boldsymbol{\delta}_i \quad (2.112)$$

Now, since the equations of conservation of momentum are in terms of force per unit volume, we divide by the volume of the control volume, V , and knowing that $\frac{NV_p}{V} = \alpha_d$:

$$\mathbf{F}'_d = \frac{F_d^p}{V} = -\frac{NV_p}{V} \sum_i \frac{\partial p}{\partial x_i} \boldsymbol{\delta}_i = -\alpha_d \nabla p \quad (2.113)$$

To summarize, the equations of conservation of mass and momentum are given below for the case of zero mass transfer between the phases:

The equation of conservation of mass for phase k:

$$\boxed{\frac{\partial(\rho_k \alpha_k)}{\partial t} + \nabla \cdot (\rho_k \alpha_k \mathbf{v}_k) = 0} \quad (2.114)$$

The equation of conservation of momentum of continuous phase:

$$\boxed{\frac{\partial(\rho_c \alpha_c \mathbf{v}_c)}{\partial t} + \nabla \cdot (\rho_c \alpha_c \mathbf{v}_c \mathbf{v}_c) = -\nabla p + \nabla \cdot \boldsymbol{\tau}_c + \alpha_c \rho_c \mathbf{g} + \mathbf{M}_c} \quad (2.115)$$

The equation of conservation of momentum of dispersed phase:

$$\boxed{\frac{\partial(\rho_d \alpha_d \mathbf{v}_d)}{\partial t} + \nabla \cdot (\rho_d \alpha_d \mathbf{v}_d \mathbf{v}_d) = \alpha_d \rho_d \mathbf{g} + \mathbf{M}_d} \quad (2.116)$$

and,

$$\boxed{\mathbf{M}_d = -\mathbf{M}_c = -\alpha_d \nabla p + \mathbf{M}'_d} \quad (2.117)$$

Substituting the above equations in the canonical form of conservation of momentum of continuous phase, we can further simplify the equations and for continuous phase the following equation will be obtained:

$$\frac{\partial(\rho_c \alpha_c \mathbf{v}_c)}{\partial t} + \nabla \cdot (\rho_c \alpha_c \mathbf{v}_c \mathbf{v}_c) = -(1 - \alpha_d) \nabla p + \nabla \cdot \boldsymbol{\tau}_c + \alpha_c \rho_c \mathbf{g} - \mathbf{M}'_d \quad (2.118)$$

which can be simplified to:

$$\frac{\partial(\rho_c\alpha_c\mathbf{v}_c)}{\partial t} + \nabla \cdot (\rho_c\alpha_c\mathbf{v}_c\mathbf{v}_c) = -\alpha_c\nabla p + \nabla \cdot \boldsymbol{\tau}_c + \alpha_c\rho_c\mathbf{g} - \mathbf{M}'_d \quad (2.119)$$

and for the dispersed phase, the conservation of momentum equation is as follows:

$$\frac{\partial(\rho_d\alpha_d\mathbf{v}_d)}{\partial t} + \nabla \cdot (\rho_d\alpha_d\mathbf{v}_d\mathbf{v}_d) = -\alpha_d\nabla p + \alpha_d\rho_d\mathbf{g} + \mathbf{M}'_d \quad (2.120)$$

It is important to note that the pressure term in the dispersed phase momentum equation is not a molecular flux within the dispersed phase, as we obtained it in other methods. Rather, it is a result of the contact of dispersed phase with the continuous phase (which has a molecular flux of pressure) in the two-fluid system.

Due to the discontinuous nature of the dispersed phase, we believe this formulation has a higher physical fidelity than other formulations. Consequently, it will be the subject of additional analyses and investigations in subsequent chapters of our work, and we will run simulations using this model (which is unprecedented in the literature) and validate it with experimental results and reference solutions from standard (Ishii's) version of the two-fluid model.

Chapter 3

Interphase Momentum Exchange Terms

3.1 Introduction

In the previous chapter, we went through the derivation of the canonical form of the two-fluid model. However, the accuracy of the model is highly affected by the interphase (interfacial) momentum exchange term, \mathbf{M}_k . This term includes the momentum transfer corresponding to interactions between the phases and can be subdivided into different contributions (forces). These closures are primarily derived using empirical relations. Hence, extra care is required to prevent an adverse impact on the model accuracy since these terms happen to affect the simulation results significantly [24].

In chapter 1, we discussed the differences between the Eulerian and Lagrangian approaches for multiphase flow. In fact, one main disadvantage of the two-fluid model that challenges its accuracy is the difficulty in prescribing interphase models to capture the interactions between the phases. Unlike the Euler-Lagrange approach in which each particle is represented by its own model and set of equations, the averaging process used in the derivation of the two-fluid model results in loss of information about local instantaneous flow properties and introduction of additional unknown correlation terms, which adds complexity to the system [22]. In order to address these interactions, different interphase exchange forces, namely, drag, virtual mass, lift, *etc.*, are defined and used in the two-fluid model. However, not all the interactions between the phases can be captured using these familiar closures, and other interphase exchange terms are added depending on the flow type and regime.

Although many closures are proposed and used in multiphase flow simulations in the literature, fewer efforts have been made to validate and investigate these closures. We notice a gap between the introduction and usage of these terms in the two-fluid model. In this chapter, we will first introduce some of the well-known closures. Then we introduce and investigate three less studied closures which, unlike many others in the literature, are supported by theoretical derivations of kinetic theory.

3.2 Interphase momentum exchange

The averaging process used for the derivation of the two-fluid model results in information loss about the local flow condition specifically the hydrodynamic and hydrostatic stress around the surface of dispersed phase. Therefore, in order to restore this info and the effect of local flow on the averaged properties of flow, the interphase momentum exchange is introduced to each phase momentum equation of the two-fluid model. It is worth mentioning that a general exact two-fluid model that applies to any multiphase flow type and regime can potentially be derived if we could precisely model these additional momentum exchange terms [22]. However, the large number of multiphase model closures for each flow regime shows that we are far away from that.

To review, the momentum equation of dispersed phase is given as:

$$\frac{\partial(\rho_d\alpha_d\mathbf{v}_d)}{\partial t} + \nabla \cdot (\rho_d\alpha_d\mathbf{v}_d\mathbf{v}_d) = \alpha_d\rho_d\mathbf{g} + \mathbf{M}_d \quad (3.1)$$

and for continuous phase, we have:

$$\frac{\partial(\rho_c\alpha_c\mathbf{v}_c)}{\partial t} + \nabla \cdot (\rho_c\alpha_c\mathbf{v}_c\mathbf{v}_c) = -\nabla p + \nabla \cdot \boldsymbol{\tau}_c + \alpha_c\rho_c\mathbf{g} + \mathbf{M}_c \quad (3.2)$$

The interphase momentum exchange term is defined as follows as shown in the previous chapter:

$$\mathbf{M}_d = -\mathbf{M}_c = -\alpha_d\nabla p + \mathbf{M}'_d \quad (3.3)$$

Now, we will focus on the forces acting on the dispersed phase which is decomposed into different components:

$$\mathbf{M}'_d = \sum_i \mathbf{F}_i \quad (3.4)$$

The acting forces on the dispersed phase are drag, virtual mass, lift, interfacial pressure, and wall lubrication. Besides these five terms, we will introduce and discuss three other terms below: dispersion, bubble pressure, and effective stress.

3.2.1 Drag Force

The relative motion between the two phases brings about the drag force. Drag force has two components, skin drag, and form drag force, which are related to the imbalance of the shear stress and the pressure distribution at the surface of an immersed body caused by relative motion respectively [2]. Although separate correlations are derived for different contributions of the drag force when averaging is performed (which are given in equation 13 of chapter 2), it is common to have a single closure for the total drag force in the two-fluid model.

The simplest correlation for the drag force is given by Stokes' law derived by theoretical analysis. Using Stokes' law, the drag force for a single sphere moving through an infinite viscous fluid is given by [31]:

$$\mathbf{F}_d = 6\pi\mu_c r \mathbf{v}_r \quad (3.5)$$

where μ_c is the viscosity of the continuous phase, $\mathbf{v}_r = \mathbf{v}_c - \mathbf{v}_d$ is the relative velocity of the two phases, and r is the radius of the spherical particle. Stokes' law can achieve high accuracy for very low Reynolds number, i.e., $Re < 1$.

For higher Reynolds numbers, a closure based on scaling analysis is being used to calculate this force for a single particle/bubble [2]:

$$\mathbf{F}_d = \frac{1}{2}\rho_c A C_d |\mathbf{v}_c - \mathbf{v}_d| (\mathbf{v}_c - \mathbf{v}_d) \quad (3.6)$$

where ρ_c is the density of the fluid, A is the projected area of the particle/bubble, and C_d is the dimensionless drag coefficient.

The total average drag force per unit volume for a large number of particles is given in terms of phase fraction. For spherical particles/bubbles, the correlations is given by:

$$\mathbf{F}_d = \frac{3}{4}\rho_c \alpha_d \frac{C_D}{d_p} |\bar{\mathbf{v}}_c - \bar{\mathbf{v}}_d| (\bar{\mathbf{v}}_c - \bar{\mathbf{v}}_d) \quad (3.7)$$

where $\bar{\mathbf{v}}_r = \bar{\mathbf{v}}_c - \bar{\mathbf{v}}_d$ is the mean relative velocity and d_p is the bubble/particle diameter.

The drag coefficient is highly dependent on the characteristics of the flow and is a function of particle Reynolds number [7]:

$$Re_p = \frac{\rho_c |\bar{\mathbf{v}}_r| d_p}{\mu_c} \quad (3.8)$$

After Stokes' law, theoretical studies on the dependence of the drag coefficient (C_d) on particle Reynolds number have not progressed, given the very complex behavior of the flow

around the immersed body. That being the case, determination of drag coefficient relies on experimental studies of the flow, and the results are usually interpreted with respect to drag coefficient versus Reynolds number. An example for spherical particles in constant relative velocity is shown in Figure 3.1 [22].

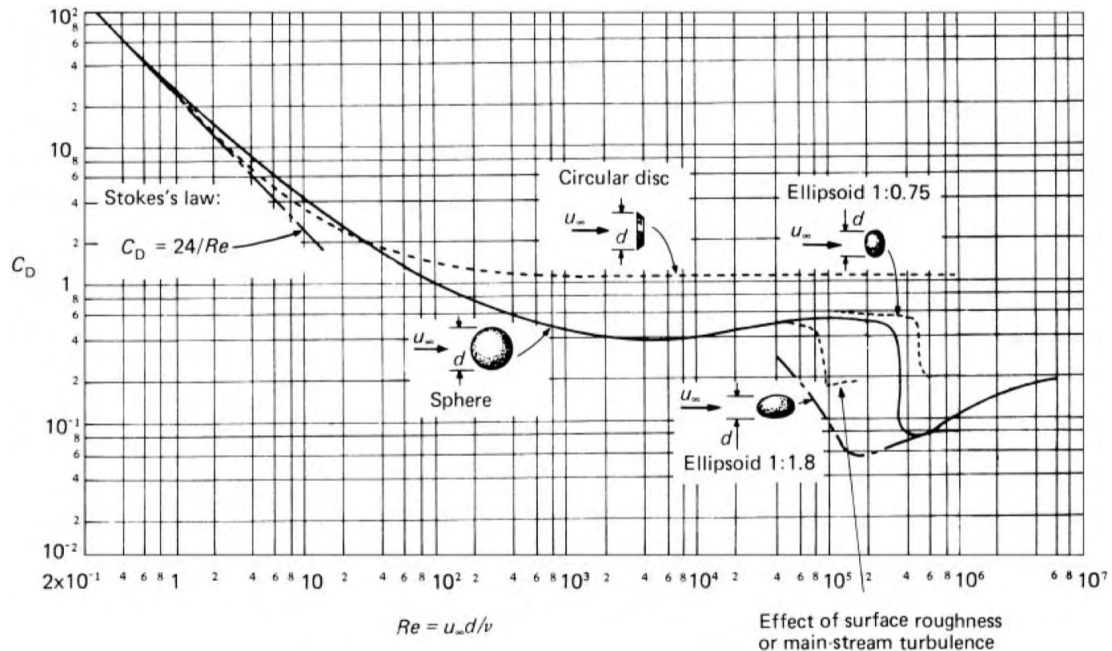


Figure 3.1: Drag coefficients of smooth, axially symmetric bodies [7]

Many different empirical relations for drag coefficient based on Reynolds number are given for different types of the dispersed phase, i.e., bubbles and solid particles based on experiments. In what follows, we will review a few of these drag coefficients.

Drag Coefficient for Bubbles and Droplets

Several different models have been proposed in the literature for the drag coefficient of bubbly flow. In this section two of the most applied models, Schiller-Naumann [32] and Ishii-Zuber [1], will be reviewed

The Schiller-Naumann model is relatively simple and is used mainly for the laminar

regime. The drag coefficient is given as follows [32, 24]:

$$C_D = \frac{24}{Re_p} (1 + 0.15Re_p^{0.687}), \quad \text{if } Re_p < 1000 \quad (3.9)$$

and for the case of Reynolds number higher than 1000, it uses a constant drag coefficient:

$$C_D = 0.44, \quad \text{if } Re_p > 1000 \quad (3.10)$$

In the Ishii-Zuber model, various regimes have been considered for drag coefficient calculation based on the characteristics of the dispersed bubbles/droplets, such as volume fraction and Reynolds number. The drag coefficient for each regime are showed in Table 3.1.

Flow Regime	Drag Coefficient (C_d)
Stokes Regime	$C_d = \frac{24}{Re_{pm}}$
Undistorted Particle Regime	$C_d = \frac{24}{Re_{pm}} (1 + 0.1Re_{pm}^{0.75})$
Distorted Particle Regime	$C_d = \frac{4d_d}{6} f(\alpha_d) \sqrt{\frac{g(\rho_c - \rho_d)}{\sigma}}$
Churn Turbulent Regime	$C_d = \frac{8}{3} (1 - \alpha_d)^2$

Table 3.1: The drag coefficient for different flow regimes [1]

One difference of the Ishii-Zuber model compared to other models is that it uses the mixture viscosity for particle Reynolds number rather than continuous phase viscosity to account for the effect of particles on the surrounding flow:

$$Re_{pm} = \frac{\rho_c |\mathbf{v}_r| d_p}{\mu_m} \quad (3.11)$$

where the mixture viscosity is defined based on maximum packing limit α_{dm} and viscosity of the continuous phase [2]:

$$\mu_m = \mu_c \left(1 - \frac{\alpha_d}{\alpha_{dm}}\right)^{-2.5\alpha_{dm}\mu^*} \quad (3.12)$$

For solid particles, $\mu^* = 1$ but for droplet/bubbles it is defined as:

$$\mu^* \equiv \frac{\mu_d + 0.4\mu_c}{\mu_d + \mu_c} \quad (3.13)$$

The function $f(\alpha_d)$ is dependent on the difference in the viscosity of both phases, and it is given by:

$$f(\alpha_d) = \begin{cases} (1 - \alpha_d)^{-0.5} & \text{for } \mu_c \gg \mu_d \\ (1 - \alpha_d)^{-1.0} & \text{for } \mu_c \approx \mu_d \\ (1 - \alpha_d)^{-1.5} & \text{for } \mu_c \ll \mu_d \end{cases} \quad (3.14)$$

Drag Coefficient for Solid Particles

For solid particles, a common model proposed by Wallis defines the drag coefficient as follows: [7]:

$$C_d = \begin{cases} \frac{24}{Re_p} (1 + 0.15Re_p^{0.687}) & \text{for } Re_p \leq 10^3 \\ 0.44 & \text{for } Re_p > 10^3 \end{cases} \quad (3.15)$$

It has been shown that for $Re_p < 10^3$, it has an accuracy of $\pm 5\%$ of experimental results [22].

3.2.2 Lift Force

Lift force is the perpendicular component of the force exerted on the particle by fluid around it due to shear force, asymmetric pressure, or the rotation of the particle itself [33, 34, 22]. Lift force is significant in gas-liquid flows in which areas with high shear rates exist, while it is far less consequential for solid-liquid flows to the point that it is considered negligible [35].

For a single spherical particle in a weak shear flow of an infinite inviscid fluid, the lift force is calculated to be as follows by Auton [36]:

$$\mathbf{F}_L = \frac{1}{2} \rho_c \mathbf{v}_r \times (\nabla \times \mathbf{v}_c) \quad (3.16)$$

Drew and Lahey derived an empirical relation for the lift force for low volume fraction in a multiphase flow which is given as [33, 37]:

$$\mathbf{F}_L = C_L \rho_c \alpha_d \mathbf{v}_r \times (\nabla \times \mathbf{v}_c) \quad (3.17)$$

where C_L is a dimensionless coefficient, and as Auton's derivation shows, it is analytically calculated to be 0.5 for a non-deformable spherical particle in an inviscid fluid [22, 2].

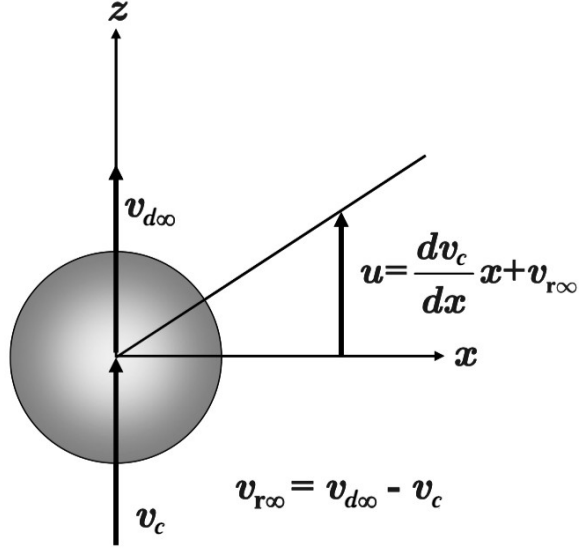


Figure 3.2: Schematic diagram of a spherical particle in a shear flow [2]

For multi-particle systems, Hibiki and Ishii proposed a correlation for the lift coefficient [2]:

$$C_L = \xi \sqrt{[C_L^{\text{lowRe}}(Re, G_s)]^2 + [C_L^{\text{highRe}}(Re)]^2} \quad (3.18)$$

where G_s is the non-dimensional velocity gradient defined using particle radius, r_d :

$$G_s \equiv \left| \frac{r_d}{v_r} \frac{dv_c}{dx} \right| \quad (3.19)$$

and ξ is a modification factor:

$$\xi = 2 - \exp(-2.92 D_d^{*2.21}) \quad (3.20)$$

$$D_d^* \equiv \frac{d_d}{4\sqrt{\sigma/g\Delta\rho}}$$

and C_L^{lowRe} and C_L^{highRe} are defined as:

$$C_L^{\text{lowRe}}(Re, G_s) = \frac{6}{\pi^2 (2Re_p G_s)^{1/2}} \frac{2.255}{(1 + 0.1Re_p/G_s)^{3/2}} \quad (3.21)$$

and,

$$C_L^{\text{highRe}}(Re) = \frac{1}{2} \left(\frac{1 + 16Re_p^{-1}}{1 + 29Re_p^{-1}} \right) \quad (3.22)$$

3.2.3 Virtual Mass Force

The virtual mass or added mass force is the additional force required to accelerate the fluid which is moving together with the particle/bubble, *i.e.*, the wake of the particle/bubble.

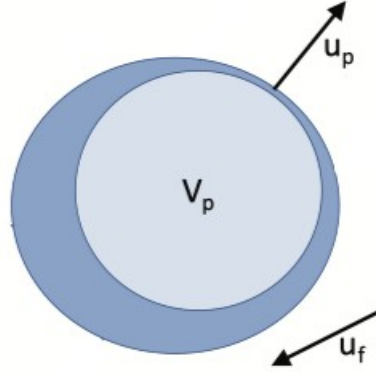


Figure 3.3: Schematic of the particle with the virtual mass added to it (the blue region) [8]

Virtual mass is significant in the gas-liquid flow, where the dispersed phase can easily be accelerated due to its low inertia. It has been shown that the virtual mass force improves the two-fluid model's numerical stability by reducing the rapid acceleration of the dispersed phase [38].

The virtual mass force for a single sphere which is accelerating in an inviscid fluid is given as follows [39, 33]:

$$\mathbf{F}_{VM} = \alpha_d \rho_c C_{VM} \left(\frac{D_d \mathbf{v}_d}{Dt} - \frac{D_c \mathbf{v}_c}{Dt} \right) \quad (3.23)$$

where C_{VM} is a dimensionless coefficient and $\frac{D_k}{Dt}$ is the material derivative with respect to phase k velocities:

$$\frac{D_k \mathbf{v}_k}{Dt} = \frac{\partial \mathbf{v}_k}{\partial t} + \mathbf{v}_k \cdot \nabla \mathbf{v}_k \quad (3.24)$$

In the case of a single non-deformable sphere, the virtual mass coefficient C_{VM} is considered to be equal to 0.5 [39].

Different virtual mass coefficients have been reported in the literature for high volume fractions of the dispersed phase. Zuber proposed a virtual mass coefficient [40, 41] is a widely used model, which gives reliable results up to large phase fraction values.

$$C_{VM} = \frac{1}{2} \left(\frac{1 + 2\alpha_d}{1 - \alpha_d} \right) \quad (3.25)$$

where $\alpha_d \rightarrow 0$, the coefficient for a single particle is derived.

Another correlation has been proposed by Van Wijngaarden [42] :

$$C_{VM} = \frac{1}{2} (1 + 2.78\alpha_d) + \mathcal{O}(\alpha_d^2) \quad (3.26)$$

3.2.4 Wall Lubrication Force

The wall lubrication force is a hydrodynamic force that pushes bubbles away from the wall in gas-liquid multiphase flow. It is caused by asymmetric drainage of the liquid around a moving bubble in the vicinity of the wall. Due to the no-slip condition of the liquid at the wall, the liquid will drain slower in the wall vicinity. As a result of this asymmetry, a force tends to move the bubbles away from the wall [2, 23]. The wall lubrication force is given as follows [43]:

$$\mathbf{F}_W = -C_W \alpha_d \rho_c |\mathbf{v}_r - (\mathbf{v}_r \cdot \mathbf{n}_W) \mathbf{n}_W|^2 \mathbf{n}_W \quad (3.27)$$

where \mathbf{n}_W is the outward unit normal of the wall, and C_W is the wall coefficient. The wall coefficient is defined as [43, 44]:

$$C_W = \max \left\{ 0, \frac{C_{W1}}{d_b} + \frac{C_{W2}}{y_W} \right\} \quad (3.28)$$

where y_W is the distance from the wall, d_b is the bubble diameter, and C_{W1} and C_{W2} are constants with the values of $C_{W1} = -0.01$ and $C_{W2} = 0.05$.

Figure 3.4 shows the effect of C_{W1} and C_{W2} on the wall force and compares it with experimental results in a pipeline [45]. In Figure 3.5, schematic comparison of the different interfacial forces and how they act on the dispersed phase is shown.

3.2.5 Interfacial Pressure

One of the terms that is obtained in derivation of the two-fluid model from volume/time averaging is the interfacial pressure difference as shown in Equations 2.51 and 2.19:

$$(p_k^{int} - p_k) \nabla \alpha_k \quad (3.29)$$

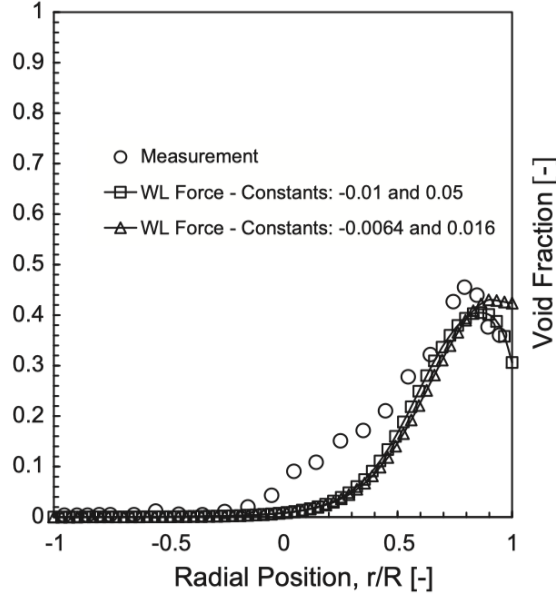


Figure 3.4: Effect of the wall lubrication force on volume fraction (α_d): Comparison between the simulation and experimental results

where p_k is the average bulk pressure and p_k^{int} is the interfacial averaged pressure of the phase k . Since $\nabla\alpha_c = -\nabla\alpha_d$, this term is usually written in terms of dispersed phase volume fraction and added as an interphase momentum exchange term:

$$\mathbf{F}_p = (p_k^{int} - p_k) \nabla\alpha_d \quad (3.30)$$

The average interfacial pressure can be derived using the pressure distribution relative to the bulk pressure. This process involves making a few assumptions and approximations. While the interfacial pressure difference for the gas phase is negligible [43], Stuhmiller proposed closure for p_c^{int} assuming that the pressure of both phases is equal, $p_c = p_d$, based on Bernoulli's law that the pressure varies with the square of velocity along a streamline and potential flow solution for flow around a sphere [38]:

$$p_c^{int} = p_c - C_p \rho_c |\mathbf{v}_r|^2 \quad (3.31)$$

where C_p is the interfacial pressure coefficient. By neglecting viscous forces, Stuhmiller derived the following interfacial pressure coefficient [38]:

$$C_p = 0.37C_d \quad (3.32)$$

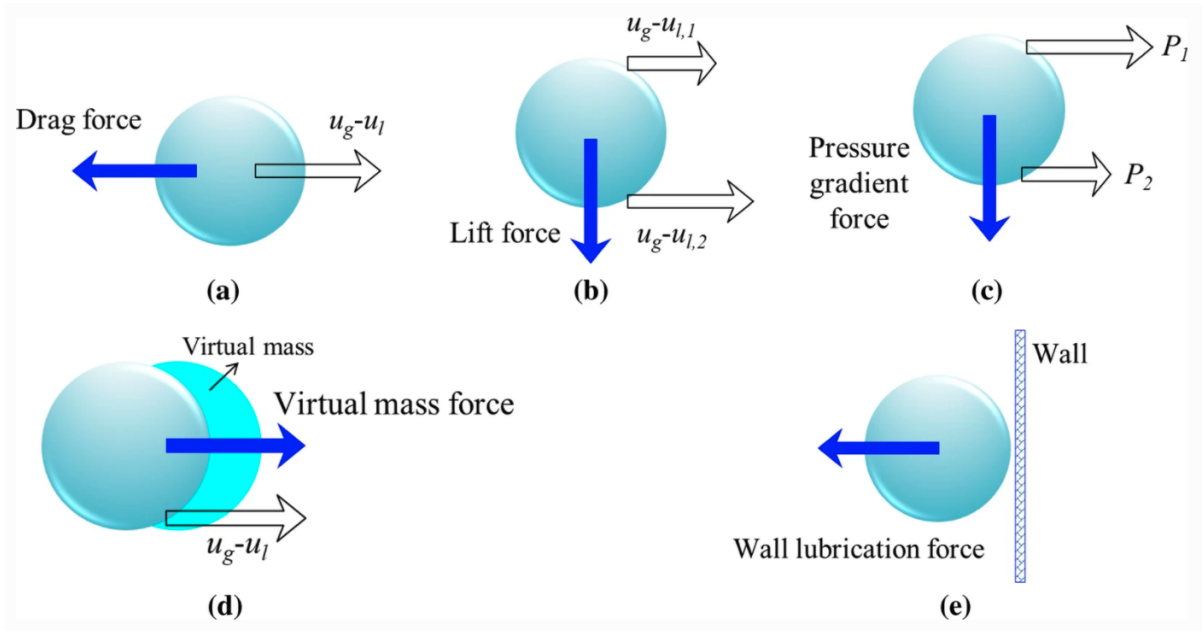


Figure 3.5: Schematic of the a)drag, b)lift, c)pressure gradient, d)virtual mass, e)wall lubrication force on the dispersed phase. [9]

where C_d is the drag coefficient. Therefore, the following closure for the interfacial pressure force can be obtained:

$$\mathbf{F}_p = -0.37\rho_c C_D |\mathbf{v}_r|^2 \nabla \alpha_d \quad (3.33)$$

It has been shown that the inclusion of the interfacial pressure as a momentum exchange term can improve the stability of the numerical solution by making the equations hyperbolic [38].

3.3 Kinetic Theory-Based Closures

Kinetic theory of gases is one approach to derive the two-fluid model, as shown in chapter 2. The derivation of the two-fluid model usually involves several assumptions and simplifications since the kinetic theory is mostly used for derivation of the two-fluid model for the inviscid dispersed phase.

Bieshuevel et al. [46] tried to derive the momentum equation for bubbles as dispersed phase and came up with the following equations in terms of local instantaneous properties

which is similar to Gidaspow derivation [20] as shown in chapter 2:

$$\frac{\partial(\alpha_d \rho_d \mathbf{v}_d)}{\partial t} + \nabla \cdot (\alpha_d \rho_d \mathbf{v}_d \mathbf{v}_d) - \nabla \cdot (\boldsymbol{\pi}_d + \boldsymbol{\pi}_c) = \alpha_d \rho_d \mathbf{F} \quad (3.34)$$

where \mathbf{F} accounts for the drag, virtual mass, buoyancy force, and $\boldsymbol{\pi}_d$ is the stress exerted on the bubble. The $\boldsymbol{\pi}_c$ term is the kinetic contribution to the stress tensor of a continuous phase which is defined in terms of the probability density function of the number of bubbles.

It is very challenging, if not impossible, to give a rigorous derivation of these stresses for the system of interest. As a result, Biesheuvel et al. used phenomenological reasoning and the kinetic theory framework to come up with reasonable closure for the stresses to close the momentum equation of the dispersed phase [46]. In the next section, we will introduce and review these closures originally derived for the case in which the continuous phase is a liquid, and the dispersed phase is bubbles. However, these closures are extendable to the solid particle dispersed phase as well.

3.3.1 Bubble Pressure and Effective Stress

In the two-phase system of interest, the presence of a liquid continuous phase causes a pressure gradient which can increase the mean bubble momentum. Additionally, it brings about a stress that acts on the surface of the bubble. To understand these forces better, imagine a control volume that moves along with the mean velocity of the bubbles inside it. In order to stop bubbles from entering or leaving the control volume due to their velocity fluctuations, a force should be exerted by the materials outside of the control volume.

Part of this force is acted on the control volume and comes from the transient pressure distribution which is related to the mean square of the velocity fluctuations. Using the pressure definition in the kinetic theory, Biesheuvel proposed the following correlation for this kinetic contribution and called it bubble pressure [46]:

$$p_{bp} = \alpha_d (\rho_d + \rho_c C_{VM}) \overline{\Delta \mathbf{v}^2} \quad (3.35)$$

where $\overline{\Delta \mathbf{v}^2}$ is the bubble mean square of the velocity fluctuations. Batchelor suggested the following correlation for it [47]:

$$\begin{aligned} \overline{\Delta \mathbf{v}^2}(\alpha_d) &= H(\alpha_d) |\mathbf{v}_c - \mathbf{v}_d|^2 \\ H(\alpha_d) &= \frac{\alpha_d}{\alpha_{cp}} \left(1 - \frac{\alpha_d}{\alpha_{cp}} \right) \end{aligned} \quad (3.36)$$

where α_{cp} is the volume fraction of the dispersed phase in the close-packing limit, and it is considered to be 0.63 for the solid particles and 1 for bubbles. In the limits that $\alpha_d \rightarrow 0$ and $\alpha_d \rightarrow \alpha_{cp}$, the velocity fluctuations go to zero, which is reasonable physically. Therefore, the final closure for the bubble pressure term is given as follows [46, 12]:

$$p_{bp} = \alpha_d (\rho_d + \rho_c C_{VM}) H(\alpha_d) |\mathbf{v}_c - \mathbf{v}_d|^2 \quad (3.37)$$

The momentum exchange associated with this pressure that is added to the momentum equation is given by:

$$F_{bp} = \nabla p_{bp} = \nabla [\alpha_d (\rho_d + \rho_c C_{VM}) H(\alpha_d) |\mathbf{v}_c - \mathbf{v}_d|^2] \quad (3.38)$$

It is noteworthy that in the kinetic theory of gases, pressure is the force exerted by the particles (atoms) hitting the walls of the container. It is obtained using Newton's second law of motion and is proportional to the mean squared velocity of particles:

$$P = \frac{Nm\overline{\mathbf{v}^2}}{3V} \quad (3.39)$$

where N is the number of particles, V is the volume of container, and $\overline{\mathbf{v}^2}$ is the average squared velocity of particles defined as:

$$\overline{\mathbf{v}^2} = \overline{\mathbf{v}_x^2} + \overline{\mathbf{v}_y^2} + \overline{\mathbf{v}_z^2} \quad (3.40)$$

$$\overline{\mathbf{v}_x^2} = \overline{\mathbf{v}_y^2} = \overline{\mathbf{v}_z^2} \quad (3.41)$$

The other part of the force acts on the bubbles within the control volume to overcome the attractive and repulsive forces between the bubbles. This contribution originates from the dynamic pressure distribution at the surface of the bubbles. This force results in an exchange of momentum which is through the fluid around the bubble surface, and consequently, it is proportional to the size of the bubble. Using the kinetic theory framework, this force is associated with effective stress and is proportional to an effective viscosity. Based on the similarity of effective diffusivity for mass and the effective kinematic viscosity for momentum, Batchelor proposed the following closure for effective kinematic viscosity [47, 46, 12]:

$$\nu_{d,\text{eff}} = C_{\text{eff}} d_p |\mathbf{v}_c - \mathbf{u}_d| \sqrt{H(\alpha_d)} \quad (3.42)$$

where C_{eff} is a constant of $\mathcal{O}(1)$. Consequently, the effective viscosity is obtained as follows [46]:

$$\mu_{d,\text{eff}} = \alpha_d (\rho_d + C_{VM} \rho_c) \nu_{d,\text{eff}} \quad (3.43)$$

Knowing the effective viscosity, the momentum exchange associated with that is derived similar to the molecular viscosity, which is through adding the divergence of the effective stress term given as follows for Newtonian fluids:

$$\boldsymbol{\tau}_{d,\text{eff}} = \mu_{d,\text{eff}} [\boldsymbol{\nabla} \mathbf{v}_d + (\boldsymbol{\nabla} \mathbf{v}_d)^T] \quad (3.44)$$

When effective viscosity is used for the dispersed phase, the viscosity of the continuous phase should also be modified, and an effective viscosity for the continuous phase which is the summation of effective viscosity of the dispersed phase and the molecular viscosity of the continuous phase is used for the continuous phase [48].

The bubble pressure term can act as a driving force that moves bubbles from areas with higher volume fractions to areas of lower. As a result, it can improve the stability of the numerical solution of the two-fluid model [48].

3.3.2 Dispersion Force

In this section, we will introduce and discuss another closure term for the two-fluid model. The turbulent dispersion force which arises due to turbulent fluctuations of liquid velocity has been well studied in the literature [49]. However, a less studied but important force that is also present in the laminar flow emanates from the microscale fluctuations of dispersed phase velocity that affects macroscale flow and is called the dispersion force. In addition to momentum flux, dispersion gives rise to a mass flux which could be added to the conservation of mass equations.

The dispersion force originates from the diffusive flux of dispersed phase particles due to fluctuations in their velocity. This force captures the hydrodynamic interactions between them through the continuous phase [46, 10]. The diffusive flux of bubbles (dispersed phase generally) caused by the fluctuating motion in 1-dimension is equal to:

$$- \delta_{d,\text{eff}}(\alpha_d) \frac{\partial n}{\partial z} \quad (3.45)$$

where $\delta_{d,\text{eff}}$ is the effective diffusivity of the bubbles and is given as follows:

$$\delta_{d,\text{eff}} = C_{\text{dis}} d_p |\mathbf{v}_c - \mathbf{u}_d| \sqrt{H(\alpha_d)} \quad (3.46)$$

where n is the number of bubbles per unit volume and C_{dis} is a constant of $\mathcal{O}(1)$ commonly considered equal to 1.3 in the literature [10]. Owing to this diffusive flux, the mean velocity of bubbles will change, which will affect the drag force.

The change in the mean bubble velocity is equal to [46]:

$$-\frac{\delta_{d,\text{eff}}(\alpha_d)}{n} \frac{\partial n}{\partial z} \quad (3.47)$$

It can be easily shown that the volume fraction is equal to the number per unit volume multiplied by the volume of the bubbles assuming a constant bubble size:

$$V_p \times n = \alpha_d \quad (3.48)$$

using this equations and by writing down the equation in 3 dimensions, the change in mean bubble velocity is given as follows:

$$-\frac{\delta_{d,\text{eff}}(\alpha_d)}{\alpha_d} \nabla \alpha_d \quad (3.49)$$

In order to obtain the momentum exchange due to the dispersion term, the impact of change in the mean bubble velocity on drag force should be derived [46]. Hence, Equation 3.7 will be used to derive the dispersion force:

$$\mathbf{F}_{dis} = \frac{3}{4} \frac{C_D}{d_p} \frac{\rho_c}{\alpha_c} \delta_{d,\text{eff}}(\alpha_d) |\mathbf{v}_c - \mathbf{v}_d| \nabla \alpha_d \quad (3.50)$$

which after substituting the value for effective diffusivity, yields [10]:

$$\mathbf{F}_{dis} = \frac{3}{4} C_D C_{dis} \frac{\rho_c}{\alpha_c} \sqrt{H(\alpha_d)} |\mathbf{v}_c - \mathbf{v}_d|^2 \nabla \alpha_d \quad (3.51)$$

The dispersion force acts as a driving force that diffuses bubbles from areas with higher volume fractions to areas with lower volume fractions. Consequently, smoother volume fraction and numerical stability can be achieved when dispersion is added to the simulations of the two-fluid model by removing the sharp changes in volume fraction. In addition, the introduction of dispersion force brings about numerical stability by making the two-fluid model conditionally hyperbolic, [10] which is the subject of more discussion in the next chapter.

Contribution to the Conservation of Mass

The diffusive mass flux due to the fluctuating motion of dispersed phase can be calculated using the effective diffusivity [46]:

$$-\delta_{d,\text{eff}} \nabla n \quad (3.52)$$

where n is the number density of dispersed phase particles which is defined as number of particles per unit volume:

$$n = \frac{N}{V} \quad (3.53)$$

Multiplying Equation 3.52 by the volume of particles, V_p , we get the diffusive flux in terms of volume fraction since $\alpha_d = nV_p$:

$$- \delta_{d,\text{eff}} \nabla \alpha_d \quad (3.54)$$

The divergence of this term can be added to the incompressible conservation of mass equation from Chapter 2 which results in:

$$\frac{\partial \alpha_d}{\partial t} + \nabla \cdot (\alpha_d \mathbf{v}_d) - \nabla \cdot (\delta_{d,\text{eff}} \nabla \alpha_d) = 0 \quad (3.55)$$

This is subject to more studies in Chapter 4, and the mass dispersion term and its significance will be analyzed using scaling analysis.

Chapter 4

Scaling Analysis of Closure Terms

4.1 Closures derived based on kinetic theory

In the previous chapter, we discussed different closure terms used in the two-fluid model and their importance for the accuracy of capturing the interaction between the phases and, as a result, the model. The last three closures, bubble pressure, effective stress, and dispersion forces, have one similar thing in common and their existence is supported by the theoretical analysis of the kinetic theory of gasses. This chapter will perform further analysis on these three closures to determine the significance of these closures for common multiphase flow regimes. The three multiphase flow regimes considered for the study in this chapter are:

- Bubbly Flow
- Liquid/Dispersed Microorganism Flow
- Particulate Flow

These are the most prevalent types of flow in the industry, and they are present in bubble columns, pipelines, chemical reactors, bioreactors, and fluidized bed reactors. Gaseous bubbles are present in bubbly flow in which there is a dispersion of gas bubbles in the liquid. Examples of the second particle type are bacteria and cells present in bioreactors. Lastly, solid particles are present in the form of catalysts, precipitates, or crystals in different industries.

In order to compare the order of magnitude of these closures, we will use scaling analysis and the typical values of parameters in each of these flow types, including the velocity, size, and density of dispersed phase particles which are given in table 4.1. The scaling parameter for the spatial coordinate is assumed to be $z_s = 1$ and since we have the assumption of low velocity of the continuous phase, the scaling parameter of both relative velocity and dispersed phase velocity is the same \mathbf{v}_{rs} .

Dispersed Particle Type	Relative velocity(m/s)	Diameter of particles(m)	Density (kg/m ³)
Gaseous Bubbles	10 ⁻¹	10 ⁻³	1
Microorganisms	10 ⁻³	10 ⁻⁵	10 ³
Solid Particles	10 ⁻²	10 ⁻³	10 ³

Table 4.1: Properties of the dispersed phase in different flow regimes

The first step of our analysis will be non-dimensionalizing the equations of conservation of mass and momentum for the dispersed phase. Then we will use the typical order of magnitude of the aforementioned parameters and determine the significance of each closure for the three flow types.

Since the three closures are derived and introduced by Biesheuvel *et al.* [46], we will use the conservation of momentum equation they proposed for the dispersed phase, which uses Stokes' law for the drag force. For the conservation of mass equation, we will add the diffusive flux of mass dispersion and determine its significance compared to the convection term. These equations are given below:

Conservation of mass:

$$\frac{\partial \alpha_d}{\partial t} + \nabla \cdot (\alpha_d \mathbf{v}_d) - \nabla \cdot (\delta_{d,\text{eff}} \nabla \alpha_d) = 0 \quad (4.1)$$

Conservation of momentum:

$$\frac{\partial}{\partial t} (\alpha_d \rho_d \mathbf{v}_d) + \nabla \cdot (\alpha_d \rho_d \mathbf{v}_d \mathbf{v}_d) = -\nabla p_{bp} + \nabla \cdot (\mu_e \nabla \mathbf{v}_d) - \alpha_d C_D (\mathbf{v}_r + \frac{\delta_{d,\text{eff}}}{\alpha_d} \nabla \alpha_d) + \alpha_d (\rho_d - \rho_c) \mathbf{g} \quad (4.2)$$

where \mathbf{v}_r is the averaged relative velocity, μ_e is the effective viscosity of dispersed phase as defined in the previous chapter, and C_D is the modified Stokes drag coefficient for multiple particle flow, which is defined as follows [46]:

$$C_D = \frac{12\pi d_p \mu_c}{4/3\pi d_p^3} f_0 \quad (4.3)$$

where f_0 accounts for the effect of hydrodynamic interaction between the dispersed phase particles on the drag force, and it is defined as [46]:

$$f_0 = \frac{1}{1 - \alpha_d} \quad (4.4)$$

The bubble pressure and effective stress are the first and second term on the right-hand side of Equation 4.2 and the dispersion force is the second term in the second parenthesis of the right-hand side. We did not include the virtual mass term in the momentum equation since it is not the subject of our scaling analysis.

4.2 Conservation of Mass

In this section, the significance of the mass dispersion term will be analyzed using scaling analysis. As shown in Chapter 3, the dispersion gives rise to a mass diffusive flux of the dispersed phase for incompressible flow as shown in Equations 3.55:

$$\frac{\partial \alpha_d}{\partial t} + \nabla \cdot (\alpha_d \mathbf{v}_d) - \nabla \cdot (\delta_{d,\text{eff}} \nabla \alpha_d) = 0 \quad (4.5)$$

Using scaling analysis, the equation can be non-dimensionalized:

$$\frac{1}{t_s} \frac{\partial \alpha_d}{\partial \tilde{t}} + \frac{\mathbf{v}_{rs}}{z_s} \tilde{\nabla} \cdot (\alpha_d \tilde{\mathbf{v}}_d) - \frac{\delta_{es}}{z_s^2} \tilde{\nabla} \cdot (\delta_{d,\text{eff}} \tilde{\nabla} \alpha_d) = 0 \quad (4.6)$$

Next, we multiply the equation by t_s which is the hydrodynamic time-scale of particles:

$$\frac{\partial \alpha_d}{\partial \tilde{t}} + \tilde{\nabla} \cdot (\alpha_d \tilde{\mathbf{v}}_d) - \frac{\delta_{es}}{\mathbf{v}_{rs} z_s} \tilde{\nabla} \cdot (\delta_{d,\text{eff}} \tilde{\nabla} \alpha_d) = 0 \quad (4.7)$$

The Peclet Number, which is the ratio of advective flux to diffusive flux, is defined as

$$Pe = \frac{\mathbf{v}_{rs} z_s}{\delta_{es}} \quad (4.8)$$

Hence, Equation 4.7 can be written in terms of Peclet number:

$$\frac{\partial \alpha_d}{\partial \tilde{t}} + \tilde{\nabla} \cdot (\alpha_d \tilde{\mathbf{v}}_d) - (Pe)^{-1} \tilde{\nabla} \cdot (\delta_{d,\text{eff}} \tilde{\nabla} \alpha_d) = 0 \quad (4.9)$$

Now, using the non-dimensional form of the equation, we will determine and compare the significance of each term using the scaling parameters for each variable for the three flow regimes of interest.

4.2.1 Bubbly Flow

In order to evaluate the Peclet Number in Equation 4.7, we need to first evaluate the magnitude order of effective diffusivity scaling parameter which is referred to as δ_{es} :

$$\delta_{es} = C_{dis}d_p |\mathbf{v}_{rs}| \sqrt{H(\alpha_d)} \quad (4.10)$$

Assuming that bubble diameter is in order of 1 mm and $|\mathbf{v}_{rs}|$ and $\sqrt{H(\alpha_d)}$ are $\mathcal{O}(10^{-1})$, and C_{dis} is $\mathcal{O}(1)$:

$$\delta_{es} \sim (1)(10^{-3})(10^{-1})(10^{-1}) = 10^{-5} \quad (4.11)$$

Therefore, the order of magnitude of the diffusive term relative to the convective term can be calculated as follows:

$$\boxed{(Pe)^{-1} = \frac{10^{-5}}{(10^{-1})(1)} = 10^{-4}} \quad (4.12)$$

4.2.2 Liquid/Dispersed Microorganism Flow

The order of magnitude of effective diffusivity δ_{es} can be calculated by evaluating the following equation:

$$\delta_{es} = C_{dis}d_p |\mathbf{v}_{rs}| \sqrt{H(\alpha_d)} \quad (4.13)$$

Assuming that microorganism diameter is of order of 10^{-5} m, \mathbf{v}_{rs} is $\mathcal{O}(10^{-3})$, $H(\alpha_d)$ is $\mathcal{O}(10^{-1})$, and C_{dis} is $\mathcal{O}(1)$, the scaling parameter of effective diffusivity is calculated as follows:

$$\delta_{es} \sim (1)(10^{-5})(10^{-3})(10^{-1}) = 10^{-9} \quad (4.14)$$

Therefore, the order of magnitude of the diffusive term relative to the convective term can be calculated as follows:

$$\boxed{(Pe)^{-1} = \frac{10^{-9}}{(1)(1)} = 10^{-9}} \quad (4.15)$$

4.2.3 Particulate Flow

Assuming that solid particle's diameter is of order of 10^{-3} m, \mathbf{v}_{rs} is of order of 10^{-2} m/s, $H(\alpha_d)$ of $\mathcal{O}(10^{-1})$, and C_{dis} of $\mathcal{O}(1)$ the order of magnitude of effective diffusivity for solid particles will be:

$$\delta_{es} \sim (1)(10^{-3})(10^{-2})(10^{-1}) = 10^{-6} \quad (4.16)$$

Therefore, the inverse of the Peclet number is calculated as follows:

$$\boxed{(Pe)^{-1} = \frac{10^{-6}}{(1)(1)} = 10^{-6}} \quad (4.17)$$

Based on the above results, it can be seen that the dispersion of mass is more significant for the bubbly flow, although due to lower magnitude compared to convective flux, it is neglected for all three flow regimes in most cases [6, 46].

4.3 Conservation of Momentum

In this section, the order of magnitude of the bubble pressure, the effective stress, and the dispersion force is determined by scaling the equation of conservation of momentum. If we substitute the Stokes' drag coefficient according to Equation 4.3, the equation of conservation of momentum will be as follows:

$$\begin{aligned} \frac{\partial}{\partial t}(\alpha_d \rho_d \mathbf{v}_d) + \nabla \cdot (\alpha_d \rho_d \mathbf{v}_d \mathbf{v}_d) = & -\nabla p_{bp} + \nabla \cdot (\mu_e \nabla \mathbf{v}_d) - \frac{12\pi d_p \mu_c}{4/3\pi d_p^3} \alpha_d f_0 (\mathbf{v}_r + \frac{\delta_{d,\text{eff}}}{\alpha_d} \nabla \alpha_d) \\ & - \alpha_d (\rho_d - \rho_c) \mathbf{g} \end{aligned} \quad (4.18)$$

By scaling this equation, we have:

$$\begin{aligned} \frac{\rho_d \mathbf{v}_{rs}}{t_s} \frac{\partial}{\partial \tilde{t}} (\alpha_d \tilde{\mathbf{v}}_d) + \frac{\rho_d \mathbf{v}_{rs}^2}{z_s} \tilde{\nabla} \cdot (\alpha_d \tilde{\mathbf{v}}_d \tilde{\mathbf{v}}_d) = & -\frac{p_{bps}}{z_s} \tilde{\nabla} (p_{\tilde{b}p}) + \frac{\mu_{es} \mathbf{v}_{rs}}{z_s^2} \tilde{\nabla} (\tilde{\mu}_e \tilde{\nabla} \mathbf{v}_d) \\ & - \frac{9\mu_c f_0 \mathbf{v}_{rs}}{d_p^2} \alpha_d \tilde{\mathbf{v}}_r - \frac{9\mu_c f_0 \delta_{es}}{d_p^2 z_s} \delta_{d,\text{eff}} \tilde{\nabla} \alpha_d - g_s \alpha_d (\rho_d - \rho_c) \tilde{\mathbf{g}} \end{aligned} \quad (4.19)$$

If we multiply by $\frac{t_s}{\mathbf{v}_{rs} \rho_d}$, the non-dimensional form of the conservation of momentum will be obtained as follows:

$$\begin{aligned} \frac{\partial}{\partial \tilde{t}} (\alpha_d \tilde{\mathbf{v}}_d) + \tilde{\nabla} \cdot (\alpha_d \tilde{\mathbf{v}}_d \tilde{\mathbf{v}}_d) = & -\frac{p_{bps}}{\mathbf{v}_{rs}^2 \rho_d} \tilde{\nabla} (p_{\tilde{b}p}) + \frac{\mu_{es}}{\mathbf{v}_{rs} z_s \rho_d} \tilde{\nabla} (\tilde{\mu}_e \tilde{\nabla} \tilde{\mathbf{v}}_d) \\ & - \frac{9\mu_c f_0 z_s}{d_p^2 \rho_d \mathbf{v}_s} \alpha_d \tilde{\mathbf{v}}_{rs} - \frac{9\mu_c f_0 \delta_{es}}{d_p^2 \mathbf{v}_{rs}^2 \rho_d} \delta_{d,\text{eff}} \tilde{\nabla} \alpha_d - \frac{z_s g_s}{\mathbf{v}_{rs}^2 \rho_d} \alpha_d (\rho_d - \rho_c) \tilde{\mathbf{g}} \end{aligned} \quad (4.20)$$

Using this form of the equation, we will determine and compare the order of magnitude of the three closure terms using the assumed values for scaling parameters from Table 4.1 for the three flow regimes of interest.

4.3.1 Bubbly Flow

The assumptions that we have for the dispersed phase in bubbly flow are the relative velocity of the order of 0.1 m/s and diameter of the order of 1 mm (10^{-3} m). Based on these assumptions from the literature [50], the dimensionless coefficient of the bubble pressure, the effective stress, and the dispersion force can be calculated.

Bubble Pressure

The expression for the bubble pressure force is given as follow as shown in the chapter 3:

$$p_{bp} = \alpha_d (\rho_d + \rho_c C_{VM}) H(\alpha_d) |\mathbf{v}_c - \mathbf{v}_d|^2 \quad (4.21)$$

The scaling parameter for the bubble pressure assuming that $C_{VM} = 0.5$ and $H(\alpha_d)$ and α_d are $\mathcal{O}(10^{-1})$ is calculated as follow [46]:

$$\begin{aligned} p_{bps} &= \alpha_d (\rho_d + \rho_c C_{VM}) H(\alpha_d) |\mathbf{v}_{rs}|^2 \\ &\sim (10^{-1})(10^3)(10^{-1})(10^{-1})^2 = 10^{-1} \end{aligned} \quad (4.22)$$

Therefore, the dimensionless coefficient of the bubble pressure is calculated as follows:

$$\frac{p_{bps}}{\mathbf{v}_{rs}^2 \rho_d} \sim \frac{10^{-1}}{(10^{-1})^2 (1)} = 10^1 \quad (4.23)$$

The effective stress

The effective viscosity, μ_e , is defined as follows:

$$\mu_e = \alpha_d (\rho_d + C_{VM} \rho_c) \nu_e(\alpha_d) \quad (4.24)$$

In order to determine its magnitude, we first need to calculate the scaling parameter of effective kinematic viscosity, assuming that C_{eff} is $\mathcal{O}(1)$, it can be calculated as follows:

$$\nu_{es}(\alpha_d) = C_{\text{eff}} d_p |\mathbf{v}_{rs}| \sqrt{H(\alpha_d)} \sim (1)(10^{-3})(10^{-1})(10^{-1}) = 10^{-5} \quad (4.25)$$

Therefore, the scaling parameter for the effective viscosity is equal to:

$$\mu_{es} \sim (10^{-1})(10^3)(10^{-5}) = 10^{-3} \quad (4.26)$$

Consequently, the dimensionless coefficient of effective stress term which shows its significance is equal to:

$$\frac{\mu_{es}}{\mathbf{v}_{rs} \rho_d z_s} \sim \frac{10^{-3}}{(10^{-1})(1)(1)} = 10^{-2} \quad (4.27)$$

The dispersion force

From Equation 4.20, the definition of the dispersion force using the Stokes' drag law is given as follows [46]:

$$\frac{9\mu_c f_0 \delta_{es}}{d_p^2 \mathbf{v}_{rs}^2 \rho_d} \delta_{d,\text{eff}} \tilde{\nabla} \alpha_d \quad (4.28)$$

As shown in the Equation 4.11, the magnitude of δ_{es} is 10^{-5} for bubbly flow and based on the definition, $f_0 \sim 1$. Thus, the dimensionless coefficient of the dispersion term is equal to:

$$\frac{9\mu_c f_0 \delta_{es}}{d_p^2 \mathbf{v}_{rs}^2 \rho_d} \sim \frac{(10)(10^{-3})(1)(10^{-5})}{(10^{-3})^2 (10^{-1})^2 (1)} = 10 \quad (4.29)$$

The drag force

In order to benchmark these closures, their magnitude can be compared to the drag force which is calculate based on the Stokes' drag:

$$\frac{9\mu_c f_0 z_s}{d_p^2 \rho_d \mathbf{v}_{rs}} \sim \frac{(10)(10^{-3})(1)(1)}{(10^{-3})^2 (1)(10^{-1})} = 10^5 \quad (4.30)$$

Molecular viscosity term

In order to make a comparison, in this section we will compare these closures to the viscous tensor for incompressible Newtonian fluid. The viscous stress definition is given by [31]:

$$\boldsymbol{\tau}_d = -\mu_d (\boldsymbol{\nabla} \mathbf{v}_d + \boldsymbol{\nabla} \mathbf{v}_d^T) \quad (4.31)$$

Now we scale this equation and derive:

$$\boldsymbol{\nabla} \cdot \tilde{\boldsymbol{\tau}}_d = \frac{(\mu_d)(\mathbf{v}_{rs})}{z_s^2} \tilde{\nabla} \cdot (\tilde{\nabla} \tilde{\mathbf{v}}_d + \tilde{\nabla} \tilde{\mathbf{v}}_d^T) \quad (4.32)$$

Since we multiply the equation of conservation of momentum by $\frac{t_s}{v_{rs} \rho_d}$ the coefficient of viscous stress term would be:

$$\frac{\mu_d}{\mathbf{v}_{rs} \rho_d z_s} \quad (4.33)$$

Therefore, using the viscosity of air for dispersed phase ($\mu_d \sim 10^{-5}$), the order of magnitude of the viscous stress tensor can be calculated as follows:

$$\frac{\mu_d}{\mathbf{v}_{rs} \rho_d z_s} \sim \frac{10^{-5}}{(10^{-1})(1)(1)} = 10^{-4} \quad (4.34)$$

4.3.2 Liquid/Dispersed Microorganism Flow

The assumptions that we have for microorganisms are the relative velocity of order of 10^{-3} m/s, size order of $d_p = 10 \mu\text{m} = 10^{-5}$ m, and density of $\mathcal{O}(10^3)$ [51, 52]. Based on these assumptions from the literature, we will evaluate the three closures.

The bubble pressure

Using Equation 4.21 as the definition of bubble pressure, and assuming that $\alpha_d \sim 10^{-1}$, the scaling parameter can be calculated as follows:

$$\begin{aligned} p_{bps} &= \alpha_d (\rho_d + \rho_c C_{VM}) H(\alpha_d) |\mathbf{v}_{rs}|^2 \\ &\sim (10^{-1})(10^3)(10^{-1})(10^{-3})^2 = 10^{-5} \end{aligned} \quad (4.35)$$

Therefore, the order of magnitude of the bubble pressure is calculated as follows:

$$\frac{p_{bps}}{\mathbf{v}_{rs}^2 \rho_d} \sim \frac{10^{-5}}{(10^{-3})^2 (10^3)} = 10^{-2} \quad (4.36)$$

The effective stress

The effective viscosity, μ_e , is defined as:

$$\mu_e = \alpha_d (\rho_d + C_{VM} \rho_c) \nu_e(\alpha_d) \quad (4.37)$$

In order to determine its magnitude, we first need to calculate the scaling parameter of effective kinematic viscosity, assuming that C_{eff} is $\mathcal{O}(1)$, it can be calculated as follows:

$$\nu_{es}(\alpha_d) = C_{\text{eff}} d_p |\mathbf{v}_{rs}| \sqrt{H(\alpha_d)} \sim (1)(10^{-5})(10^{-3})(10^{-1}) = 10^{-9} \quad (4.38)$$

Therefore, the scaling parameter for the effective viscosity is equal to:

$$\mu_{es} \sim (10^{-1})(10^3)(10^{-9}) = 10^{-7} \quad (4.39)$$

Consequently, the dimensionless coefficient of effective stress term which shows its significance is equal to:

$$\frac{\mu_{es}}{\mathbf{v}_{rs} \rho_d z_s} \sim \frac{10^{-7}}{(10^{-3})(10^3)(1)} = 10^{-7} \quad (4.40)$$

The dispersion force

From Equation 4.20, the definition of the dispersion force using the Stokes' drag law is given as follows [46]:

$$\frac{9\mu_c f_0 \delta_{es}}{d_p^2 \mathbf{v}_{rs}^2 \rho_d} \delta_{d,\text{eff}} \tilde{\nabla} \alpha_d \quad (4.41)$$

As shown in the Equation 4.14, the magnitude of δ_{es} is 10^{-9} for flow of microorganism in a liquid. Thus, the dimensionless coefficient of the dispersion force is equal to:

$$\frac{9\mu_c f_0 \delta_{es}}{d_p^2 \mathbf{v}_{rs}^2 \rho_d} \sim \frac{(10)(10^{-3})(1)(10^{-9})}{(10^{-5})^2 (10^{-3})^2 (10^3)} = 10^2 \quad (4.42)$$

The drag force

In order to benchmark these closure, their magnitude can be compared to the drag force which is calculate based on the Stokes' drag law:

$$\frac{9\mu_c f_0 z_s}{d_p^2 \rho_d \mathbf{v}_{rs}} \sim \frac{(10)(10^{-3})(1)(1)}{(10^{-5})^2 (10^3)(10^{-3})} = 10^8 \quad (4.43)$$

4.3.3 Particulate Flow

The assumptions for solid particles are relative velocity of order $\sim 10^{-2}$ m/s, size order of $d_p \sim 1 \text{ mm} = 10^{-3}$ m, and density of order $\sim 10^3$ [53, 54]. Based on these assumptions, magnitude of the bubble pressure, the effective stress, and the dispersion force will be evaluated.

The bubble pressure

Using Equation 4.21 as the definition of bubble pressure, the scaling parameter can be calculated as follows assuming that $\alpha_d \sim 10^{-1}$:

$$\begin{aligned} p_{bps} &= \alpha_d (\rho_d + \rho_c C_{VM}) H(\alpha_d) |\mathbf{v}_{rs}|^2 \\ &\sim (10^{-1})(10^3)(10^{-1})(10^{-2})^2 = 10^{-3} \end{aligned} \quad (4.44)$$

Therefore, the dimensionless coefficient of the bubble pressure is calculated as follows:

$$\frac{p_{bps}}{\mathbf{v}_{rs}^2 \rho_d} \sim \frac{10^{-3}}{(10^{-3})^2 (10^3)} = 10^{-3} \quad (4.45)$$

The effective stress

In order to determine the magnitude of effective stress, we first need to calculate the scaling parameter of effective kinematic viscosity, which is given below:

$$\nu_{es}(\alpha_d) = C_{\text{eff}} d_p |\mathbf{v}_{rs}| \sqrt{H(\alpha_d)} \sim (1)(10^{-3})(10^{-2})(10^{-1}) = 10^{-6} \quad (4.46)$$

Therefore, the scaling parameter for the effective viscosity is equal to:

$$\mu_{es} \sim (10^{-1})(10^3)(10^{-6}) = 10^{-4} \quad (4.47)$$

Consequently, the dimensionless coefficient of effective stress term which shows its significance is equal to:

$$\frac{\mu_{es}}{\mathbf{v}_{rs} \rho_d z_s} \sim \frac{10^{-4}}{(10^{-2})(1)(10^3)} = 10^{-5} \quad (4.48)$$

The dispersion force

As shown in Equation 4.16, the magnitude of δ_{es} is 10^{-6} for particulate flow. Thus, using Equation 4.20 the dimensionless coefficient of the dispersion force is equal to:

$$\frac{9\mu_c f_0 \delta_{es}}{d_p^2 \mathbf{v}_{rs}^2 \rho_d} \sim \frac{(10)(10^{-3})(1)(10^{-6})}{(10^{-3})^2 (10^{-2})^2 (10^3)} = 10^{-1} \quad (4.49)$$

The drag force

In order to benchmark these closures, their magnitude can be compared to the drag force which is calculated based on the Stokes' drag law:

$$\frac{9\mu_c f_0 z_s}{d_p^2 \rho_d \mathbf{v}_{rs}} \sim \frac{(10)(10^{-3})(1)(1)}{(10^{-3})^2 (10^3)(10^{-2})} = 10^3 \quad (4.50)$$

4.4 Discussion of Scaling Analysis Results

This section will further discuss the scaling analysis results for the three closures in the conservation of momentum. This will allow us to determine the most significant of the closures and incorporate it into the two-fluid model for simulations.

Table 4.2 shows the summary of scaling analysis results. Each column of this table shows the order of magnitude of each of the three closures along with the drag force and viscous stress (only for the gaseous dispersed phase).

Dispersed Particle Type	Bubble Pressure	Effective Stress	Dispersion	Drag	Viscous Stress
Gaseous Bubbles	10	10^{-2}	10	10^5	10^{-4}
Microorganisms	10^{-2}	10^{-7}	10²	10^8	-
Solid Particles	10^{-3}	10^{-5}	10⁻¹	10^3	-

Table 4.2: The order of magnitude of closure terms in different multiphase flow regimes

Based on the scaling analysis results, the dispersion force is the most significant between the three closures of interest overall for the three multiphase flow regimes. The variation in the magnitude of the three closures is less for the bubbly flow, but for microorganisms and particulate flow, the difference is more evident. Thus, based on the scaling analysis results, the dispersion should be selected to incorporate in the model as an interphase momentum exchange term.

However, the inclusion of dispersion force is not only supported by the scaling analysis, but it can also bring about other benefits such as hyperbolicity or well-posedness of the two-fluid model and as a result numerical stability and accuracy [10, 55].

Panicker *et al.* showed that the inclusion of dispersion force makes the standard version of the two-fluid model conditionally hyperbolic by admitting real eigenvalues to the system of partial differential equations. For the case that the virtual mass force is neglected, the following correlation will assure the well-posedness of the two-fluid model [10]:

$$\frac{3}{4}C_D C_{\text{dis}} \geq \frac{\rho_d (1 - \alpha_d) \sqrt{\alpha_d (1 - \alpha_d)}}{\rho_d (1 - \alpha_d) + \rho_c \alpha_d} \quad (4.51)$$

By adding the dispersion force to Brennen’s two-fluid model, which will be used for the rest of the study, we were able to verify that the two-fluid model is unconditionally well-posed if only drag is included and the dispersed phase pressure term (which is an interphase momentum exchange) is neglected.

Other than well-posedness, the dispersion force improves the stability of the numerical solution by removing the nonphysical behavior across the discontinuity and areas with high gradients in the volume fraction of the dispersed phase, especially with mesh refinement [10]. Figure 4.1 shows the results of simulations in a bubble column with and without the dispersion force from the literature [10]. The incorporation of the dispersion force results

in smoother volume fraction field and removes the sharp changes in the volume fraction which agrees more with the experimental observations.

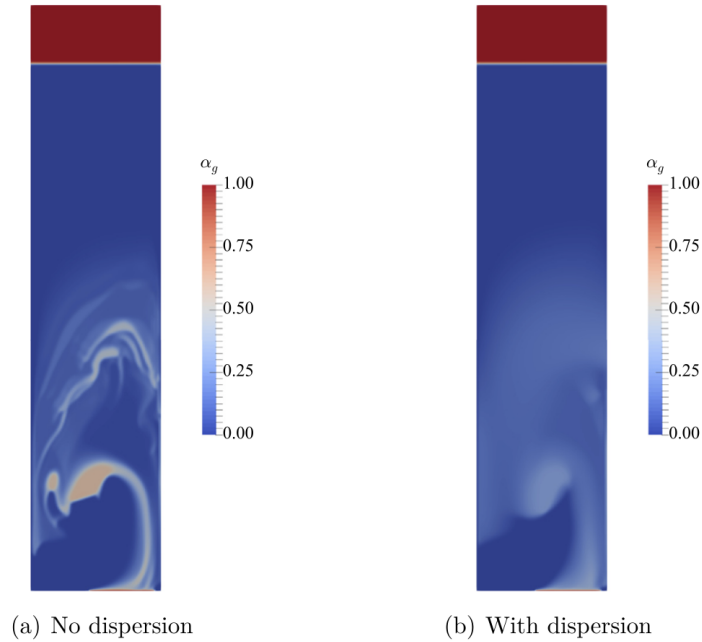


Figure 4.1: Volume fraction results in a bubble column with and without the dispersion force. [10]

In conclusion, the dispersion force showed to be the most significant between the three investigated closures. In addition, it can admit well-posedness of the two-fluid model which can remove the artifacts in the solution when mesh is refined, and brings about numerical stability and accuracy [10, 55]. Therefore, this force will be adopted in Brennen's two-fluid model [21] in the next chapter of this work. This specific version of two-fluid model will be used to run simulations and compare the results with reference solutions from the standard version (Ishii's) of the two-fluid model and validate them with experimental results.

Chapter 5

Results and Validation

This chapter introduces the proposed form of the two-fluid model based on the analysis and discussion from the previous chapters, which uses Brennen’s canonical form of the two-fluid [21] model and the dispersion force as an interphase momentum transfer term [46]. Subsequently, this model is validated with Pflieger experimental results and a reference solutions which is `twoPhaseEulerFoam` solver from `OpenFOAM` [56]. In order to achieve that, a test case is introduced, and then simulations are run for this test case using Finite Volume Method (FVM) and by modifying the `twoPhaseEulerFoam` solver in `OpenFOAM`.

5.1 The final form of the two-fluid model

To summarize the results from previous chapters, the two-fluid model used in this chapter is given below:

Conservation of mass (phase k):

$$\frac{\partial(\rho_k\alpha_k)}{\partial t} + \nabla \cdot (\rho_k\alpha_k\mathbf{v}_k) = 0 \quad (5.1)$$

Conservation of momentum (dispersed phase):

$$\frac{\partial(\rho_d\alpha_d\mathbf{v}_d)}{\partial t} + \nabla \cdot (\rho_d\alpha_d\mathbf{v}_d\mathbf{v}_d) = \alpha_d\rho_d\mathbf{g} + \mathbf{M}_d \quad (5.2)$$

Conservation of momentum (continuous phase):

$$\frac{\partial(\rho_c \alpha_c \mathbf{v}_c)}{\partial t} + \nabla \cdot (\rho_c \alpha_c \mathbf{v}_c \mathbf{v}_c) = -\nabla p + \nabla \cdot \boldsymbol{\tau}_c + \alpha_c \rho_c \mathbf{g} + \mathbf{M}_c \quad (5.3)$$

where the interphase momentum exchange term is defined as:

$$\mathbf{M}_d = -\mathbf{M}_c = -\alpha_d \nabla p + \mathbf{M}'_d \quad (5.4)$$

and the closure terms used as interphase momentum exchange between the phases are the drag and the dispersion force:

$$\mathbf{M}'_d = \mathbf{F}_{drag} + \mathbf{F}_{dis} \quad (5.5)$$

Using the definitions from Chapter 3, we have:

$$\mathbf{M}'_d = -\frac{3}{4} \rho_c \alpha_d \frac{C_D}{d_p} |\mathbf{v}_c - \mathbf{v}_d| (\mathbf{v}_c - \mathbf{v}_d) - \frac{3}{4} C_D C_{dis} \frac{\rho_c}{\alpha_c} \sqrt{H(\alpha_d)} |\mathbf{v}_c - \mathbf{v}_d|^2 \nabla \alpha_d \quad (5.6)$$

The other equation used in solving the system of PDEs is the volume fraction constraint:

$$\alpha_c + \alpha_d = 1 \quad (5.7)$$

5.2 Test Case: Laboratory-scale bubble column

In order to validate this version of the two-fluid model, a simple test case was chosen, which is a rectangular bubble column with air-water fluid system. The bottom plate of the column has a gas sparger with eight rectangular holes for gas delivery. The holes are located in the middle of the plate. Figure 5.1 shows the bubble column configuration with a sketch of the bubble swarm.

The operating condition of the bubble column is as follows:

- Height (of liquid), width, and depth of 45, 20, and 5 cm, respectively
- Air volume flux is 48 lit/h
- Operating temperature of 25°C

To measure the experimental data, laser techniques (LDA) and image processing methods (PTV, PIV) are used.

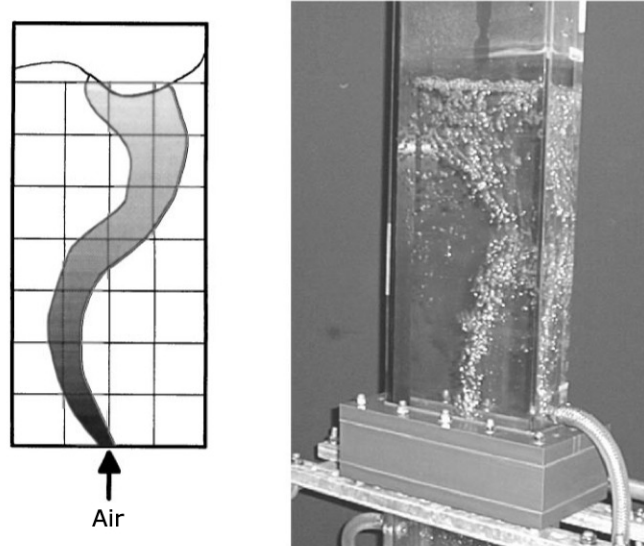


Figure 5.1: The bubble column configuration and the position of sparger [11]

5.2.1 Geometry, mesh, and simulation condition

The geometry used for the simulation and boundaries is displayed in Figure 5.2 where the blue, green, and red lines show the wall, outlet, and inlet of the domain. A column with a height of 90 cm is used, which is filled with liquid phase up to 45 cm and the rest is filled with gas. However, only the results for the section with the liquid phase are subject to study, analysis, and validation.

The drag force is included in all of the simulations in this chapter, and the Shiller-Naumann drag model [32] is used for the drag coefficient. The dispersion force is used in some of the simulations according to the definition given in Chapter 3 by Biesheuvel, [46] with a constant dispersion coefficient of 1.3. The bubble size is assumed to be 2 mm.

The case geometry was meshed using `blockMeshDict` utility of `OpenFOAM` from one of examples of `OpenQBMM` [57]. A 2-D and a 3-D mesh with hexahedral elements are created for running the simulation in both conditions.

All the reference solutions are simulated using `OpenFOAM` by `twoPhaseEulerFoam` which employs PIMPLE algorithm [58]. In order to run simulations using the proposed model, the conservation of momentum equation of dispersed phase in the `twoPhaseEulerFoam` solver is modified by using zero viscosity for the dispersed phase, and also dispersion force is added

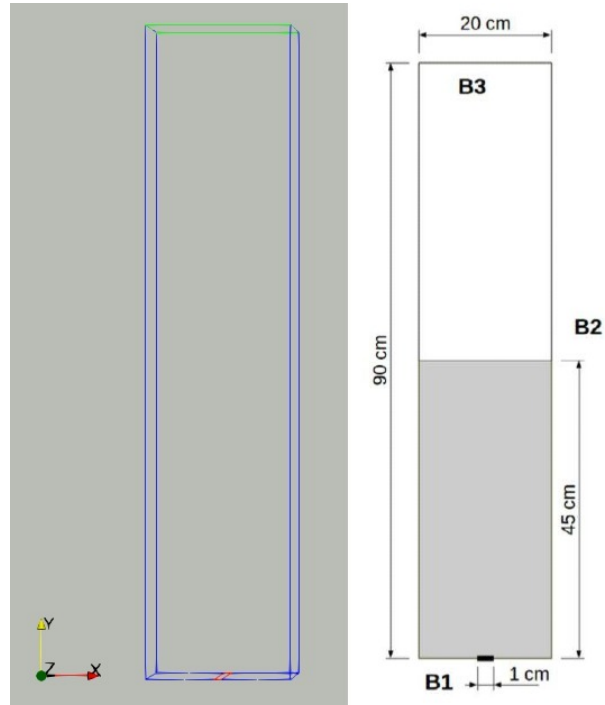


Figure 5.2: The geometry of 2-D [12] and 3-D test cases used for running simulation

as a new interphase momentum exchange term by building on the source code of `OpenFAOM`. The dispersion model is built by starting from `constantTurbulentDispersionCoefficient` which is a built-in turbulent dispersion model in `OpenFOAM` and is named `constantDispersion`. The code for this implemented model is displayed in the Appendix.

The inlet boundary condition for the velocity of both phases is a fixed value of 0 and 0.03 cm/s in the y -direction for the continuous and dispersed phase, respectively. No-slip boundary condition is used for the velocities at the walls along with zero initial value for both phases throughout the domain. For the outlet, the outflow boundary condition is used to ensure no back-flow occurs. For the volume fraction of the dispersed phase, the inlet boundary condition was a fixed value of 1 which means pure air is injected into the domain. Zero-gradient is used as the boundary condition at the walls and the outlet for the volume fraction. A pressure condition is used for the outlet set to the atmospheric pressure for the outlet. An initial time-step of 10^{-3} s was used with a maximum Courant number of 0.5.

Since the simulations are transient, the arithmetic mean of all seconds of simulation

time is calculated using the `fieldAverage` function and referred as time-averaged results in this chapter. The time-averaged value of field x for simulation run time of N is calculated as follows:

$$\bar{x} = \frac{1}{N} \sum_{i=0}^N x_i \quad (5.8)$$

where x_i is the value of the desired field at time n . In this chapter, the simulation is run for 250 s.

5.3 Comparison of 2-D simulation results with a reference solution

Since experimental results are not available for the 2-D test case, the simulation results of the model of interest are only compared with a reference solution from `twoPhaseEulerFoam` solver which uses Ishii's model. In this section, the time-averaged dispersed phase volume fraction field and vertical liquid velocities for Ishii's (standard two-fluid model) model will be shown and compared to Brennen's model (this work).

5.3.1 The dispersed phase volume fraction fields

Figure 5.3 shows the time-averaged dispersed phase volume fraction results for Ishii's and Brennen's models. The results from the two models are similar, which is supported by the scaling analysis results from Chapter 4, especially for this test case where the gas phase is diluted in most of the domain and removing the hydrodynamic stress for the dispersed phase does not affect the outcome. The other factor that leads to a negligible difference between the two models is low viscosity of the dispersed phase. It is expected to observe a more significant difference between the results obtained by the two models if the dispersed phase was also a liquid.

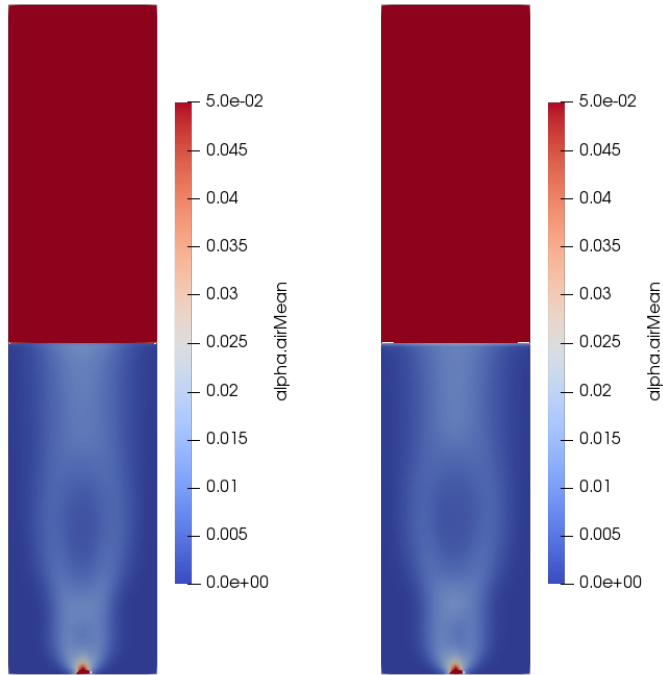


Figure 5.3: Time-averaged volume fraction field of dispersed phase: Brennen's model (left), Ishii's model (right)

5.3.2 The continuous phase vertical velocity

In this section, the vertical velocity of the continuous phase is plotted and the results are shown in Figure 5.4 for three different heights of 13, 25, and 37 cm. A similar pattern is observed for the velocities, and for all three plots, Brennen's model velocities are higher. This is indeed expected by looking at the difference between the two models. Although the viscosity of the continuous phase is unchanged, the lower velocity of the gas phase leads to higher velocities of that. As a result, the drag force between the two phases is increased and the bubbles will pull the liquid, which results in a rise in the velocity of the continuous phase for Brennen's model.

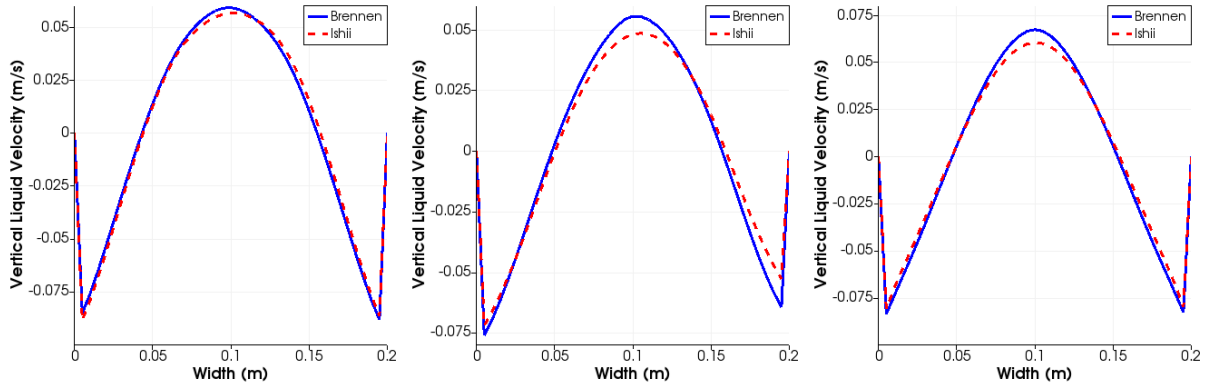


Figure 5.4: Comparison of the time-averaged continuous phase velocity at heights of 13 cm(left), 25 cm (middle), and 37 cm (right)

5.4 Validation and comparison of 3-D simulation results with a reference solution

This section will display and discuss the simulation results for the 3-D case. First, the dispersed phase volume fraction results for the two models are compared. Then, to better understand the results, vertical velocities against the width of the column are plotted for Ishii’s and Brennen’s models.

5.4.1 The dispersed phase volume fraction field without dispersion force

Figure 5.5 shows the time-averaged dispersed phase volume fraction fields for Ishii’s and Brennen’s models. The difference in the volume fraction for the two models is insignificant. One reason can be the fact that the dispersed phase is very dilute in most of the domain, and consequently, the change in its viscosity and, as a result, the viscous stress tensor of the dispersed phase does not affect the flow notably. However, by plotting the velocity results with the width of the column, a more detailed and accurate comparison between the two models can be made.

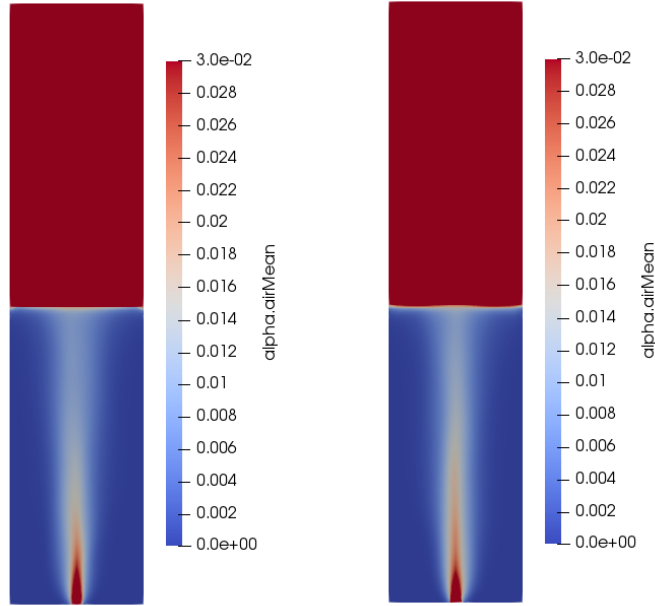


Figure 5.5: Time-averaged volume fraction field of dispersed phase: Brennen's model (left), Ishii's model (right)

5.4.2 Vertical dispersed phase velocity without dispersion force

In order to make an in-depth comparison of the results by the two models, the vertical gas velocity results are plotted for three heights (13, 25, and 37 cm) against the width of the column in Figure 5.6. The velocities obtained by Brennen's model are higher, in the middle of the column for all three heights. This is due to zero viscosity of the gas phase in Brennen's model, which results in less friction at the molecular level and, as a result, a higher velocity. Although due to the low volume fraction of the gas phase, the difference is insignificant.

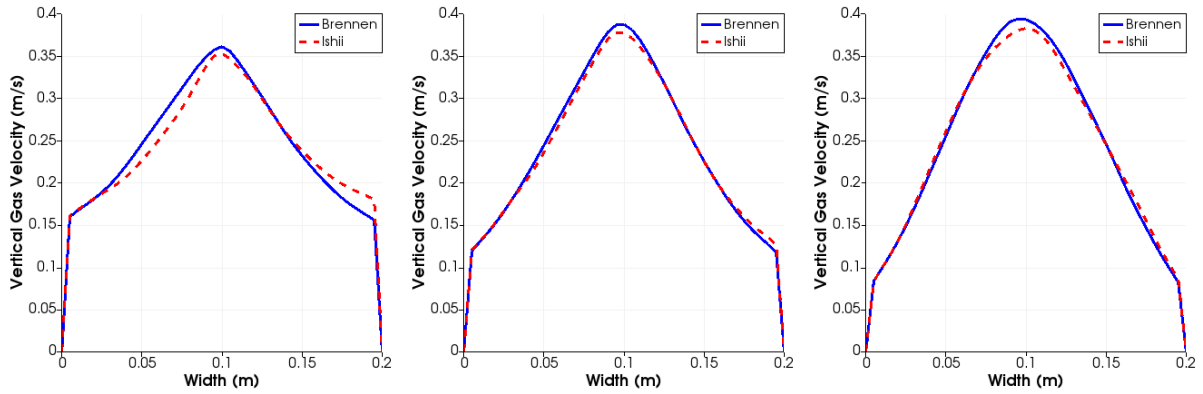


Figure 5.6: Comparison of the time-averaged dispersed phase velocity at heights of 13 cm (left), 25 cm (middle), and 37 cm (right)

5.4.3 Vertical continuous phase velocity without dispersion force

Figure 5.7 compares the results from both models by plotting the vertical liquid velocity results for the three heights against the width of the column. Brennen’s model calculates slightly higher velocities in the middle of the column which is due to the higher velocity of gas-phase and its influence on the liquid velocity by increasing the interphase momentum exchange.

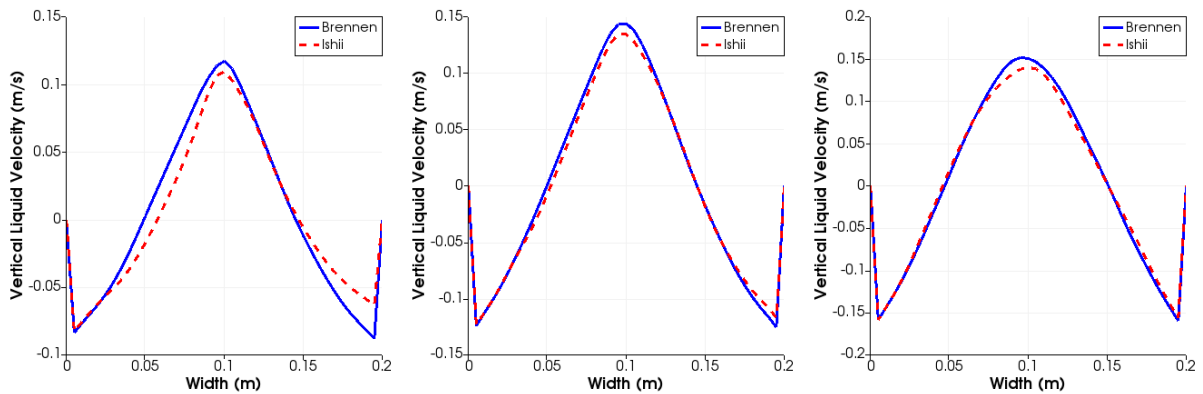


Figure 5.7: Comparison of the time-averaged continuous phase velocity at heights of 13 cm (left), 25 cm (middle), and 37 cm (right)

5.4.4 The dispersed phase volume fraction field with dispersion force

In this section, the same analysis will be done for the 3-D simulations, but this time the dispersion force is also included in the simulations. Figure 5.8 shows the dispersed phase volume fraction fields when dispersion force is incorporated into the model for Ishii's and Brennen's model. The latter obtains faintly more symmetric results and dissimilarity between the results by the two model can be observed mostly in the areas closer to the inlet.

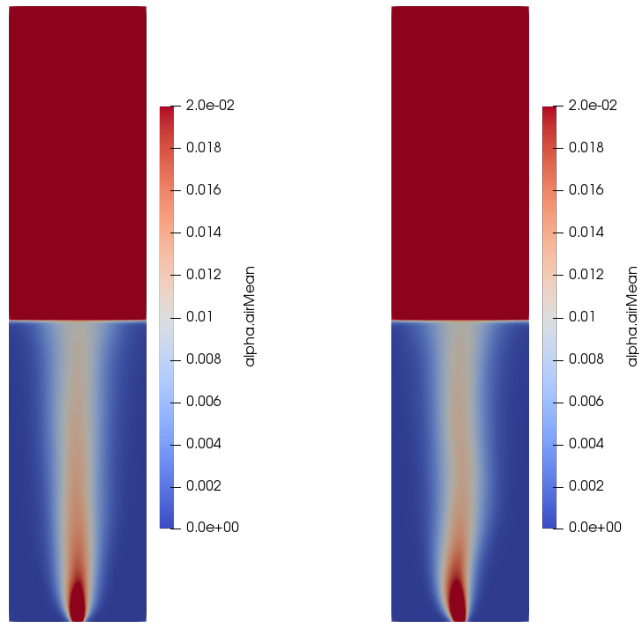


Figure 5.8: Time-averaged volume fraction field of dispersed phase: Brennen's model (left), Ishii's model (right)

5.4.5 Validation of vertical continuous phase velocity with experimental results

In this section, the results of simulations from Brennen's model, including the dispersion force, will be validated with experimental results from Pflieger test case [11]. Since the experimental results (for this test case) are available for the vertical continuous phase

velocities only, we will validate that. Figure 5.9 shows the plots of vertical liquid velocity at three heights of the column.

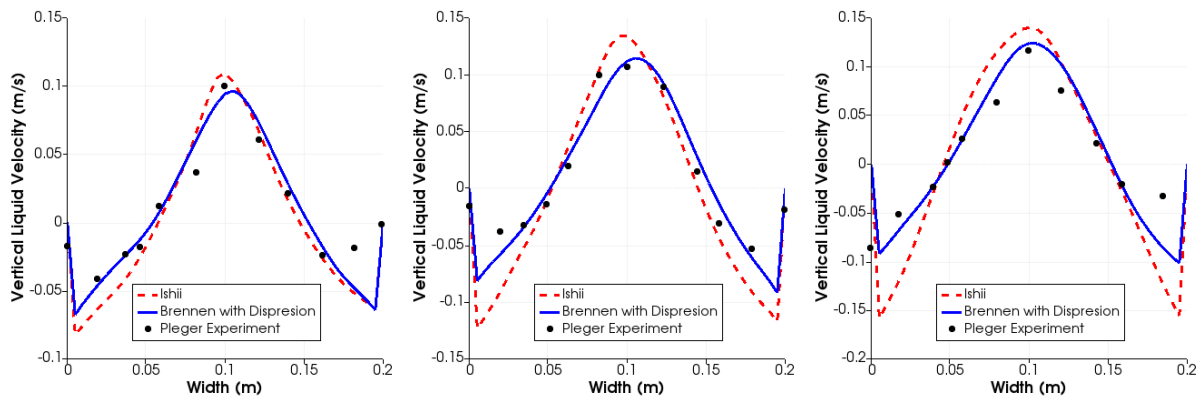


Figure 5.9: Validation of the time-averaged continuous phase velocity at heights of 13 cm (left), 25 cm (middle), and 37 cm (right)

It is discernible that generally, the results obtained by Brennen’s model plus the dispersion force have lower velocities, particularly in the middle and the areas closer to walls which has better agreement with experimental results compared to the reference solution. The results also align with the results from the literature. In [11], it has been shown that the introduction of turbulent dispersion force, which has a similar form to the dispersion force, results in lower velocity of continuous phase for this test case. Furthermore, it was illustrated In ref. [10] that addition of the dispersion force results in lower velocities of dispersed and as a results continuous phase.

This can be due to several reasons. The first factor is that when dispersion is included, due to the diffusive flux of the dispersed phase, the volume fraction of the gas phase will decrease in the middle of the column. Since the drag force is weighted by α_d , it will reduce the drag force and as a result the continuous phase velocity.

Overall, as it is evident, Brennen’s model, including the dispersion force (the model proposed by this work), has a better performance in terms of agreement with experiments and obtains significantly more accurate results than Ishii’s (standard two-fluid model).

5.5 Influence of dispersion force on simulation results

This section discusses the influence of inclusion of the dispersion force in the model. First, the influence of dispersion force on the instantaneous dispersed phase volume fraction field is examined and displayed. Subsequently, the time-averaged volume fraction field and plot of volume fraction against the width of the column at height of 25 cm are shown and discussed.

5.5.1 Instantaneous dispersed phase volume fraction field

Figure 5.10 shows the volume fraction field result obtained by Brennen's model with (right) and without (left) the dispersion force at time $t=2$ s of simulation run time. When dispersion force is introduced to the model, the nonphysical results and artifacts across the areas with the high gradient in the volume fraction of the dispersed phase are removed and smoother results are obtained. These results are expected since the dispersion force acts as a driving force that moves the gas phase from areas with higher volume fraction to lower volume fraction. Moreover, the results obtained here agree with the literature, namely the results by Panicker et al. [10].

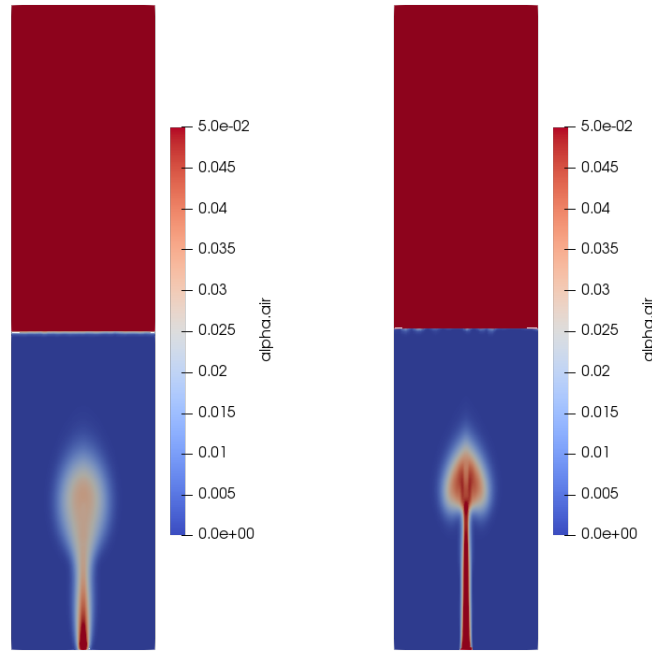


Figure 5.10: The volume fraction of dispersed phase field at the time: $t=2$ s, with (left) and without (right) dispersion force

5.5.2 Time-averaged dispersed phase volume fraction field

Figure 5.11 shows the time-averaged dispersed phase volume fraction field for the run time of 250 s. Similar to the instantaneous field, the results with the dispersion force display a lower volume fraction in the middle of the column.

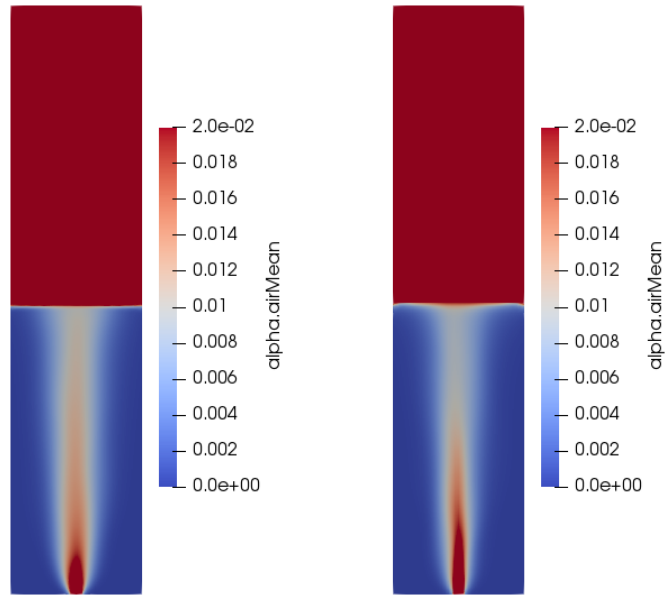


Figure 5.11: The time-averaged volume fraction of dispersed phase field with (left) and without (right) dispersion force

In order to have a better comparison, the gas volume fraction results are plotted with the width of the column at height of 25 cm in Figure 5.12. Results with the dispersion force show less variation with the width of the column which means a lower fraction in the middle and higher fraction in the areas close to the walls.

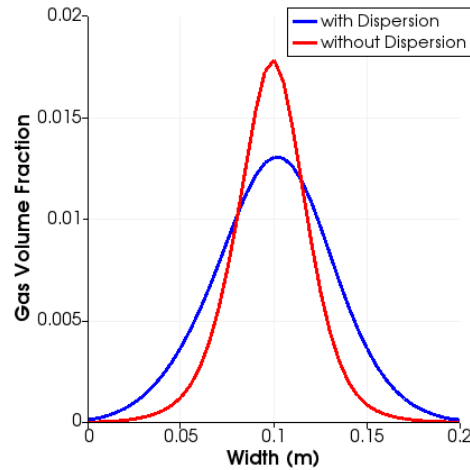


Figure 5.12: The time-averaged volume fraction of dispersed phase at height 25 cm with and without dispersion force

5.5.3 Validation of influence of dispersion force with experimental results

The influence of dispersion force on the simulation results will now be validated with experiments. In order to do that, the vertical liquid velocity computed by Brennen's model without dispersion force is compared to the results when the dispersion force is included which can be seen in Figure 5.13.

It can be seen that the results with the dispersion force agree better with the experimental results. In the author's view, two factors contribute to achieving more accurate results with the dispersion force. First, when dispersion force is included, the simulations capture the fluctuation of the dispersed phase, and the impact of these fluctuations can be considerable depending on the test case. In this case, due to the high Reynolds number, this impact seems to be significant. Secondly, the inclusion of the dispersion force potentially removes the nonphysical behavior [10] especially in the areas that gradient in volume fraction is high. Therefore, the incorporation of the dispersion force leads to more accurate simulation results.

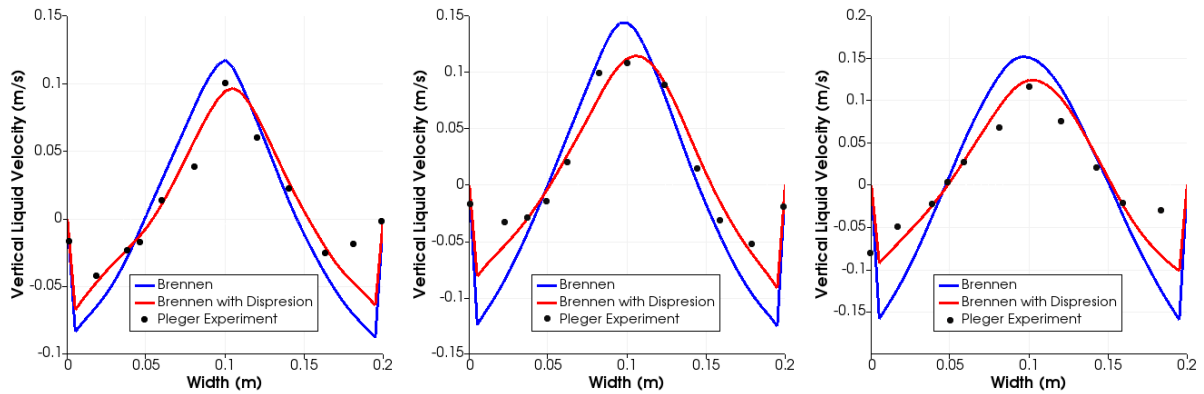


Figure 5.13: Validation of the time-averaged continuous phase velocity at heights of 13 cm (left), 25 cm (middle), and 37 cm (right) with and without dispersion force

5.6 Mesh dependency of the solutions

This section will investigate and discuss the mesh dependency of the simulation results. In order to do that, the simulations using Brennen's model, including the dispersion force, are run on a finer mesh with doubling the number of cells from 72000 to 144000. Figure 5.14 displays the gas volume fraction, vertical liquid, and gas velocity at a column height of 25 cm. Although results are close, they are not the same, and consequently, the solution is not completely mesh-independent. This is due to the sharp interface between the two phases at the column's middle height and the ill-posedness of the two-fluid model. It has been shown in [10] using higher dispersion coefficient and a different definition for $H(\alpha_d)$, the model will become well-posed and a mesh independent solution can be obtained.

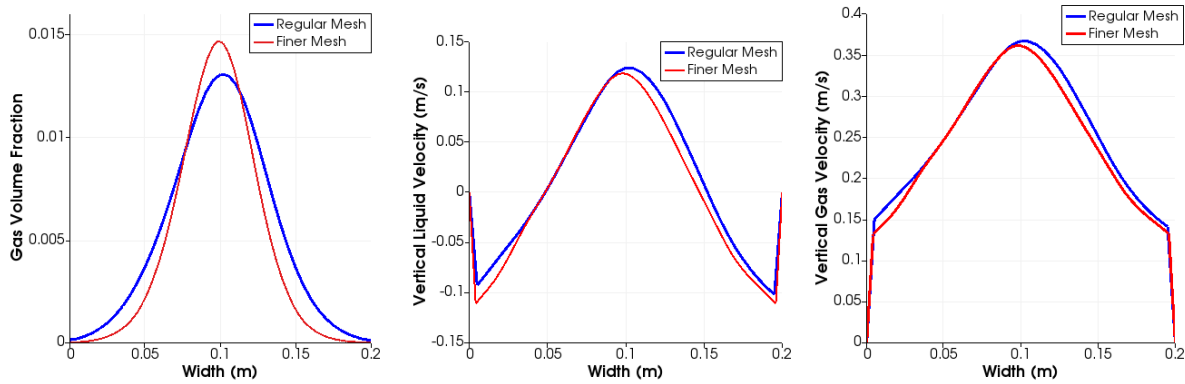


Figure 5.14: Comparison of the simulation results with mesh refinement

5.7 Summary

To validate Brennen’s two-fluid model and also the influence of the dispersion force, simulations are run for an experimental test case and compared to experiments as well as reference solutions from **OpenFOAM**. The effect of removal of dispersed phase hydrodynamic stress and also the introduction of the dispersion force on the solution are discussed. It transpired that using Brennen’s model results in slightly higher velocities of the dispersed phase and as a result, continuous phase compared to Ishii’s model. Conversely, incorporation of the dispersion force results in decrease in the volume fraction variations and also dispersed and continuous phase velocities. Consequently, the magnitude of the maximum velocity in the middle and in the areas closer to the wall decreases.

In terms of the accuracy of the results, Brennen’s model with dispersion force showed a significantly better agreement with the experimental results compared to Ishii’s model and also Brennen’s model without the dispersion force. Although for the test case discussed in this work, the difference between Ishii’s and Brennen’s models is minimal due to the low viscosity and dilute dispersed phase.

Chapter 6

Conclusion and Future Work

6.1 Conclusion

In this work, a physical model is identified, studied, investigated, and applied to simulate bubbly two-phase flow. Scaling analysis is done on three kinetic theory-based closure terms, and the most significant one is added to the model. The outcome was used for simulations of a test case, and the results are compared to the standard version of two-phase solver from `OpenFOAM` [56] as well as experimental results.

Initially, a comprehensive review of different methods of derivation of the two-fluid model is done. Then a less-studied model is introduced and studied and, due to its physical validity about the presence/absence of molecular flux in the dispersed phase, selected for validation. Subsequently, a thorough study on different closure terms used as interphase momentum exchange in the two-fluid model including three less-studied kinetic theory-based closures is conducted. Thereupon, the most significant of the three closures are determined using scaling analysis and added to the physical version (Brennen's) of the two-fluid model. Eventually, this model was employed for running simulations and validation with experimental results.

To run simulations with this model, the `twoPhaseEulerFoam` solver from `OpenFOAM` was modified to make the required changes to the canonical form and also implementing and incorporating the dispersion force.

The simulation results showed a promising outcome for the two-fluid model proposed by this work compared to the well-received standard version of the two-fluid model first proposed by Ishii [2]. For the test case studied in this work, Brennen's model with the

dispersion force achieves better accuracy in predicting the vertical velocity of the liquid phase compared to Ishii’s model.

The dispersion force was verified to bring about improvements in the stability of the numerical solution by removing the nonphysical behavior across the areas with high gradient in the volume fraction and the velocity of the dispersed phase, which aligns with the results from the literature. Therefore, smoother results for the volume fraction and the dispersed phase velocity are generated when this force is added to the simulations. Additionally, when this force is included in the standard two-fluid model, more accurate results for the velocity of the liquid phase are achieved compared to the simulation without the dispersion force.

6.2 Future Work

The main differences between the standard two-fluid model and Brennen’s model [21] used in this work is the nonexistence of viscous stress tensor for the dispersed phase in the latter. Unlike the dispersion force, which was implemented and added as an interfacial model to the `twoPhaseEulerFoam` building on the `OpenFOAM` source code, the changes to the canonical form of the model were made manually by setting the viscosity of the dispersed phase to zero. Although this approach worked for the purpose of this research, it is not the best way to implement this model. In order to have a more reliable implementation, we have been working on implementing a solver from scratch using the Finite Element Method (FEM) and Discontinuous Galerkin (DG) method, which has several benefits compared to the current FVM implementation. Even though that solver did not happen to work properly for the time frame of this research, eventually, it will be an ideal numerical solver for the resulting two-fluid model of this study.

In Chapter 5, the model is used for running simulations and validation for bubbly flow. However, it can be extended to other multiphase flow regimes, namely, particulate flow, flow of microorganisms in continuous liquid phase, and especially liquid-liquid dispersed flow, since the changes made to viscous stress of both phases in Brennen’s model in expected to show a remarkable difference in the outcome of the simulations. Hence, another recommendation for future work is to run simulations and validate the model for these flow regimes and to widen the set of validation cases of the model.

Another area of future work is adding a more diverse set of interphase momentum exchange terms to the model and also, adding the conservation of energy equations for non-isothermal cases. While only the drag and dispersion forces were considered in this work,

other momentum exchange contributions such as lift, virtual mass, and wall lubrication force can affect the simulation results if they apply to the system. However, prior to insertion into the model, a momentum exchange term must be thoroughly analyzed and proven to reflect the physics of the system; it should not be used as a way to obtain agreement with experimental results.

To summarize, the primary set of recommendations for future work are given as follows:

- **Finalize the implementation of the model using the FEM and DG:** This will result in higher-order and potentially more accurate and stable solutions, and then the solver can be added to the open-source computational multiphysics package OpenCMP [59].
- **Validation of the model for other multiphase flow regimes:** Although the model is shown to have a promising performance for a bubbly flow test case, it still needs to be examined using multiple other test cases, namely, particulate and microorganisms flow and perhaps more bubbly flow test cases.
- **Addition of other momentum exchange terms and conservation of energy to the model:** The addition of more interphase momentum exchange terms can enhance the usability and the accuracy of the model. Yet, it needs to be with prior research and analysis depending on the flow regime of interest. Moreover, adding the conservation of energy equations results in diversifying the usability of the model to a large set of non-isothermal cases.

References

- [1] Mamoru Ishii and Novak Zuber. Drag coefficient and relative velocity in bubbly, droplet or particulate flows. *AIChE Journal*, 25(5):843–855, September 1979.
- [2] Mamoru Ishii and Takashi Hibiki. *Thermo-Fluid Dynamics of Two-Phase Flow*. Springer New York, New York, NY, 2011.
- [3] J.M. Mandhane, G.A. Gregory, and K. Aziz. A flow pattern map for gas—liquid flow in horizontal pipes. *International Journal of Multiphase Flow*, 1(4):537–553, October 1974.
- [4] Ashfaq Shaikh and Muthanna H. Al-Dahhan. A Review on Flow Regime Transition in Bubble Columns. *International Journal of Chemical Reactor Engineering*, 5(1), August 2007.
- [5] Y. T. Shah, B. G. Kelkar, S. P. Godbole, and W.-D. Deckwer. Design parameters estimations for bubble column reactors. *AIChE Journal*, 28(3):353–379, May 1982.
- [6] Gilberto Espinosa-Paredes, Octavio Cazarez-Candia, Alfonso Garcia-Gutierrez, and Jeannette Martinez-Mendez. Void fraction propagation in a bubbly two-phase flow with expansion effects. *Annals of Nuclear Energy*, 29(11):1261–1298, July 2002.
- [7] B. S. Massey and A. J. Ward-Smith. *Mechanics of fluids*. Taylor & Francis, London ; New York, 8th ed edition, 2006. OCLC: ocm60321285.
- [8] Rodney O. Fox, Frédérique Laurent, and Aymeric Vié. A hyperbolic two-fluid model for compressible flows with arbitrary material-density ratios. *Journal of Fluid Mechanics*, 903:A5, November 2020.
- [9] Wei Chen and Lifeng Zhang. Effects of Interphase Forces on Multiphase Flow and Bubble Distribution in Continuous Casting Strands. *Metallurgical and Materials Transactions B*, 52(1):528–547, February 2021.

- [10] N. Panicker, A. Passalacqua, and R.O. Fox. On the hyperbolicity of the two-fluid model for gas–liquid bubbly flows. *Applied Mathematical Modelling*, 57:432–447, May 2018.
- [11] D. Pflieger, S. Gomes, N. Gilbert, and H.-G. Wagner. Hydrodynamic simulations of laboratory scale bubble columns fundamental studies of the Eulerian–Eulerian modelling approach. *Chemical Engineering Science*, 54(21):5091–5099, November 1999.
- [12] J.C. Heylmun, B. Kong, A. Passalacqua, and R.O. Fox. A quadrature-based moment method for polydisperse bubbly flows. *Computer Physics Communications*, 244:187–204, November 2019.
- [13] Clayton T. Crowe and Clayton T. Crowe, editors. *Multiphase Flow Handbook*. CRC Press, 0 edition, September 2005.
- [14] 11 Bubble Column Reactors. In *Process Systems Engineering*, volume 5, pages 327–366. Elsevier, 2002.
- [15] Th. Frank, P.J. Zwart, E. Krepper, H.-M. Prasser, and D. Lucas. Validation of CFD models for mono- and polydisperse air–water two-phase flows in pipes. *Nuclear Engineering and Design*, 238(3):647–659, March 2008.
- [16] R.I. Issa and M.H.W. Kempf. Simulation of slug flow in horizontal and nearly horizontal pipes with the two-fluid model. *International Journal of Multiphase Flow*, 29(1):69–95, January 2003.
- [17] Xu Wang, Jie Ding, Wan-Qian Guo, and Nan-Qi Ren. A hydrodynamics–reaction kinetics coupled model for evaluating bioreactors derived from CFD simulation. *Biore-source Technology*, 101(24):9749–9757, December 2010.
- [18] Hui Pan, Xi-Zhong Chen, Xiao-Fei Liang, Li-Tao Zhu, and Zheng-Hong Luo. CFD simulations of gas–liquid–solid flow in fluidized bed reactors — A review. *Powder Technology*, 299:235–258, October 2016.
- [19] Daniele L. Marchisio and Rodney O. Fox, editors. *Multiphase Reacting Flows: Modelling and Simulation*, volume 492 of *CISM International Centre for Mechanical Sciences*. Springer Vienna, Vienna, 2007.
- [20] Dimitri Gidaspow. *Multiphase flow and fluidization: continuum and kinetic theory descriptions*. Academic Press, Boston, 1994.

- [21] Christopher E. Brennen. *Fundamentals of multiphase flow*. Cambridge University Press, Cambridge [England] ; New York, 2005.
- [22] David Paul Hill. *The computer simulation of dispersed two-phase flow*. PhD thesis, Citeseer, 1998.
- [23] Treeratanaphitak, Tanyakarn. *Diffuse Solid-Fluid Interface Method for Dispersed Multiphase Flows*. PhD Thesis, UWSpace, 2018.
- [24] Mandar V. Tabib, Swarnendu A. Roy, and Jyeshtharaj B. Joshi. CFD simulation of bubble column—An analysis of interphase forces and turbulence models. *Chemical Engineering Journal*, 139(3):589–614, June 2008.
- [25] Guan Heng Yeoh, Chi Pok Cheung, and Jiyuan Tu. *Multiphase flow analysis using population balance modeling: bubbles, drops, and particles*. IChemE. Elsevier, Butterworth-Heinemann, Amsterdam, 2014.
- [26] Donald A. Drew and Stephen L. Passman. *Theory of multicomponent fluids*, volume 135. Springer Science & Business Media, 2006.
- [27] Stephen Whitaker. Diffusion and dispersion in porous media. *AIChE Journal*, 13(3):420–427, May 1967.
- [28] John C. Slattery. Flow of viscoelastic fluids through porous media. *AIChE Journal*, 13(6):1066–1071, November 1967.
- [29] Frederick A. Howes and Stephen Whitaker. The spatial averaging theorem revisited. *Chemical engineering science*, 40(8):1387–1392, 1985. ISBN: 0009-2509 Publisher: Elsevier.
- [30] Sydney Chapman and T. G. Cowling. *The mathematical theory of non-uniform gases: an account of the kinetic theory of viscosity, thermal conduction, and diffusion in gases*. Cambridge mathematical library. Cambridge University Press, Cambridge ; New York, 3rd ed edition, 1990.
- [31] Robert Byron Bird, Warren E. Stewart, and Edwin N. Lightfoot. *Transport phenomena*. Wiley, New York, revised ed edition, 2007.
- [32] Links Schiller. A drag coefficient correlation. *Zeit. Ver. Deutsch. Ing.*, 77:318–320, 1933.

- [33] D.A. Drew and R.T. Lahey. The virtual mass and lift force on a sphere in rotating and straining inviscid flow. *International Journal of Multiphase Flow*, 13(1):113–121, January 1987.
- [34] Akio Tomiyama, Hidesada Tamai, Iztok Zun, and Shigeo Hosokawa. Transverse migration of single bubbles in simple shear flows. *Chemical Engineering Science*, 57(11):1849–1858, June 2002.
- [35] Spyridon Politis. Prediction of two-phase solid-liquid turbulent flow in stirred vessels. 1989. Publisher: Imperial College London (University of London).
- [36] T. R. Auton. The lift force on a spherical body in a rotational flow. *Journal of Fluid Mechanics*, 183:199–218, October 1987.
- [37] Donald A. Drew. Analytical modeling of multiphase flow. *Particulate two-phase flow*, 1993. Publisher: Butterworth-Heinemann.
- [38] J.H. Stuhmiller. The influence of interfacial pressure forces on the character of two-phase flow model equations. *International Journal of Multiphase Flow*, 3(6):551–560, December 1977.
- [39] D. Drew, L. Cheng, and R.T. Lahey. The analysis of virtual mass effects in two-phase flow. *International Journal of Multiphase Flow*, 5(4):233–242, August 1979.
- [40] N. Zuber. On the dispersed two-phase flow in the laminar flow regime. *Chemical Engineering Science*, 19(11):897–917, November 1964.
- [41] P. D. Mineev, U. Lange, and K. Nandakumar. A comparative study of two-phase flow models relevant to bubble column dynamics. *Journal of Fluid Mechanics*, 394:73–96, September 1999.
- [42] L. Van Wijngaarden and D. J. Jeffrey. Hydrodynamic interaction between gas bubbles in liquid. *Journal of Fluid Mechanics*, 77(1):27–44, September 1976.
- [43] S.P. Antal, R.T. Lahey, and J.E. Flaherty. Analysis of phase distribution in fully developed laminar bubbly two-phase flow. *International Journal of Multiphase Flow*, 17(5):635–652, September 1991.
- [44] Th. Frank, P.J. Zwart, E. Krepper, H.-M. Prasser, and D. Lucas. Validation of CFD models for mono- and polydisperse air–water two-phase flows in pipes. *Nuclear Engineering and Design*, 238(3):647–659, March 2008.

- [45] G.H. Yeoh, Sherman C.P. Cheung, and J.Y. Tu. On the prediction of the phase distribution of bubbly flow in a horizontal pipe. *Chemical Engineering Research and Design*, 90(1):40–51, January 2012.
- [46] A. Biesheuvel and W.C.M. Gorissen. Void fraction disturbances in a uniform bubbly fluid. *International Journal of Multiphase Flow*, 16(2):211–231, March 1990.
- [47] G. K. Batchelor. A new theory of the instability of a uniform fluidized bed. *Journal of Fluid Mechanics*, 193:75–110, 1988. ISBN: 1469-7645 Publisher: Cambridge University Press.
- [48] Deify Law, Francine Battaglia, and Theodore J. Heindel. Model validation for low and high superficial gas velocity bubble column flows. *Chemical Engineering Science*, 63(18):4605–4616, September 2008.
- [49] D. Lucas, E. Krepper, and H.-M. Prasser. Use of models for lift, wall and turbulent dispersion forces acting on bubbles for poly-disperse flows. *Chemical Engineering Science*, 62(15):4146–4157, August 2007.
- [50] Li Zheng and Poojitha D. Yapa. Buoyant Velocity of Spherical and Non-spherical Bubbles/Droplets. *Journal of Hydraulic Engineering*, 126(11):852–854, 2000. eprint: <https://ascelibrary.org/doi/pdf/10.1061/%28ASCE%290733-9429%282000%29126%3A11%28852%29>.
- [51] W. J. Kowalski, William P. Bahnfleth, and T. S. Whittam. Filtration of airborne microorganisms: modeling and prediction. *Ashrae Trans*, 105:4–17, 1999. ISBN: 0001-2505.
- [52] Entezari, Kimia. Simulation-based Design of Bioreactors Using Computational Multiphysics. Master’s thesis, UWSpace, 2021.
- [53] Ali Adnan. Pilot-scale study of phosphorus recovery through struvite crystallization. 2003. Publisher: The University of British Columbia.
- [54] Kristell S. Le Corre, Eugenia Valsami-Jones, Phil Hobbs, and Simon A. Parsons. Phosphorus recovery from wastewater by struvite crystallization: A review. *Critical Reviews in Environmental Science and Technology*, 39(6):433–477, 2009. ISBN: 1064-3389 Publisher: Taylor & Francis.
- [55] Kyle Booker. H(div)-conforming Discontinuous Galerkin Methods for Multiphase Flow. May 2021. Accepted: 2021-05-05T15:09:49Z Publisher: University of Waterloo.

- [56] OpenFOAM | Free CFD Software | The OpenFOAM Foundation.
- [57] Alberto Passalacqua, Jeff Heylmun, Matteo Icardi, Ehsan Madadi, Pete Bachant, Xiaofei Hu, and Joe Weaver. OpenQBMM/OpenQBMM: OpenQBMM 7.0.0 for OpenFOAM v2106, June 2021.
- [58] Paulo J. Oliveira and R. I. Issa. AN IMPROVED PISO ALGORITHM FOR THE COMPUTATION OF BUOYANCY-DRIVEN FLOWS. *Numerical Heat Transfer Part B-fundamentals*, 40:473–493, 2001.
- [59] Monte, Elizabeth. OpenCMP: An Open-Source Computational Multiphysics Package. Master’s thesis, UWSpace, 2021.

Appendix A

Source Code

A.1 Constant Dispersion Model

```
1 /*-----*\
2  ===== |
3  \\      /  F ield      | OpenFOAM: The Open Source CFD Toolbox
4  \\      /  O peration  | Website:  https://openfoam.org
5  \\      /  A nd        | Copyright (C) 2014-2018 OpenFOAM Foundation
6  \\/      M anipulation |
7  -----*
8 License
9   This file is part of OpenFOAM modified by Mehrdad Khezrian to
   implement the Dispersion Force for two-fluid model.
10
11   OpenFOAM is free software: you can redistribute it and/or modify it
12   under the terms of the GNU General Public License as published by
13   the Free Software Foundation, either version 3 of the License, or
14   (at your option) any later version.
15
16   OpenFOAM is distributed in the hope that it will be useful, but
   WITHOUT
17   ANY WARRANTY; without even the implied warranty of MERCHANTABILITY or
18   FITNESS FOR A PARTICULAR PURPOSE. See the GNU General Public License
19   for more details.
20
21   You should have received a copy of the GNU General Public License
22   along with OpenFOAM. If not, see <http://www.gnu.org/licenses/>.
23
24 /*-----*/
```

```

25
26 #include "constantDispersion.H"
27 #include "phasePair.H"
28 #include "PhaseCompressibleTurbulenceModel.H"
29 #include "addToRunTimeSelectionTable.H"
30
31 #include "dragModel.H"
32
33 // * * * * * Static Data Members * * * * * //
34
35 namespace Foam
36 {
37     namespace turbulentDispersionModels
38     {
39         defineTypeNameAndDebug(constantDispersion, 0);
40         addToRunTimeSelectionTable
41         (
42             turbulentDispersionModel,
43             constantDispersion,
44             dictionary
45         );
46     }
47 }
48
49
50 // * * * * * Constructors * * * * * //
51
52 Foam::turbulentDispersionModels::constantDispersion::constantDispersion
53 (
54     const dictionary& dict,
55     const phasePair& pair
56 )
57 :
58     turbulentDispersionModel(dict, pair),
59     Ctd_("Ctd", dimless, dict)
60 {}
61
62
63 // * * * * * Destructor * * * * * //
64
65 Foam::turbulentDispersionModels::constantDispersion::~~constantDispersion
66 (
67     )
68 {}

```

```

69 // * * * * * Member Functions * * * * * //
70
71 Foam::tmp<Foam::volScalarField>
72 Foam::turbulentDispersionModels::constantDispersion::D() const
73 {
74     const fvMesh& mesh(pair_.phase1().mesh());
75     const dragModel&
76         drag
77         (
78             mesh.lookupObject<dragModel>
79             (
80                 IOobject::groupName(dragModel::typeName, pair_.name())
81             )
82         );
83
84     return
85         0.75
86         *Ctd_
87         *drag.CdRe()
88         *pair_.continuous().nu()
89         *pair_.continuous().rho()
90         /pair_.dispersed().d()
91         *pair_.magUr()
92         *(
93             1.0/max(pair_.continuous(), 0.001)
94         )
95         *sqrt(pair_.continuous()*pair_.dispersed());
96 }
97
98
99 // * * * * * //

```